nature communications

Article

https://doi.org/10.1038/s41467-025-57294-8

Dual-function regulator MexL as a target to control phenazines production and pathogenesis of *Pseudomonas aeruginosa*

Received: 13 May 2024

Accepted: 18 February 2025

Published online: 26 February 2025

Check for updates

Zhaoxiao Yu[1,2], Zhikun Wu[3,4], Dejian Liu[1,2], Haoyu Liu[5], Yu Zhang[1], Yaqian Zheng[1,2], Yanhong Huang[5], Shumin Liao[5], Yu Wei[4], Wei Huang[3,4,6], Zhenyu Zhang[1,2], Xi Liu[1], Haiying Yu[1], Di Wang[1], Liang Li[5], Feng Long[3,4] ✉ & Luyan Z. Ma[1,2] ✉

Antibiotic resistance or tolerance of pathogens has become one of the global public crises. Finding new drug targets may open up a way of infection control. Phenazine pyocyanin (PYO) is an important virulence factor produced by the pathogen *Pseudomonas aeruginosa*. Here we show that a multidrug efflux pump repressor, MexL, acts as a transcriptional activator to enhance phenazines production via binding with a conserved DNA motif within the promoters of phenazines biosynthesis genes. Moreover, PYO functions as a self-regulating ligand of MexL for restricting its own production and the *mexL* knockout attenuates the virulence and antibiotics tolerance of *P. aeruginosa*. Based on the structure of MexL we resolve, we find two antimicrobials that can interact with MexL to reduce the PYO production and virulence of *P. aeruginosa*. Our in vivo studies suggest that the antimicrobials combination by using MexL-antagonists to reduce bacterial virulence and enhance the efficacy of common antibiotics can be an effective way to combat *P. aeruginosa* infection.

Antibiotic resistance or tolerance of pathogens is one of the most serious global public health threats[1]. Targeting virulence has been proposed to be a paradigm for antimicrobial therapy[2]. *Pseudomonas aeruginosa* is an opportunistic pathogen that can cause life-threatening infections in immune-compromised individuals and patients with cystic fibrosis[3]. *P. aeruginosa* infections are notoriously difficult to be eradicated due to the ability of this bacterium to tolerate antibiotic treatment at the individual-cell level or through the formation of biofilms[4,5]. This opportunistic pathogen has been listed by the World Health Organization in the group of high priority pathogens that are required for research and development of new antibiotics[6]. Pyocyanin (PYO), one of the well-studied phenazines, is a secreted colorful redox-active pigment produced by *P. aeruginosa*[7,8]. This blue-green pigment, is an important virulent factor of *P. aeruginosa* that mediates tissue damage and necrosis during lung infection[9]. PYO has been reported to have a broad-spectrum antibiotic activity against other microbes, which enhances the survival of *P. aeruginosa* in a multiple-microbe environment[10–13]. Studies have reported various physiological roles of PYO, such as facilitating biofilm development, influencing iron acquisition, and serving as a signaling compound, etc[14–16]. A recent report has revealed that antibiotic tolerance can be induced by the antibiotic-triggered accumulation of PYO in *P. aeruginosa* culture[17]. Costa et al. have shown that *P. aeruginosa* biofilms can be inhibited

[1]State Key Laboratory of Microbial Resources, Institute of Microbiology, Chinese Academy of Sciences, Beijing, China. [2]University of Chinese Academy of Sciences, Beijing, China. [3]Department of neurosurgery, Zhongnan Hospital of Wuhan University, School of Pharmaceutical Sciences, Wuhan University, Wuhan, China. [4]Ministry of Education Key Laboratory of Combinatorial Biosynthesis and Drug Discovery, School of Pharmaceutical Sciences, Wuhan University, Wuhan, China. [5]Department of Pharmacology, Joint Laboratory of Guangdong-Hong Kong Universities for Vascular Homeostasis and Diseases, School of Medicine, Southern University of Science and Technology, Shenzhen, China. [6]Hubei Key Laboratory of Resources and Chemistry of Chinese Medicine, College of Pharmacy, Hubei University of Chinese Medicine, Wuhan, China. ✉e-mail: longfe@whu.edu.cn; luyanma27@im.ac.cn

https://doi.org/10.1038/s41467-025-57294-8

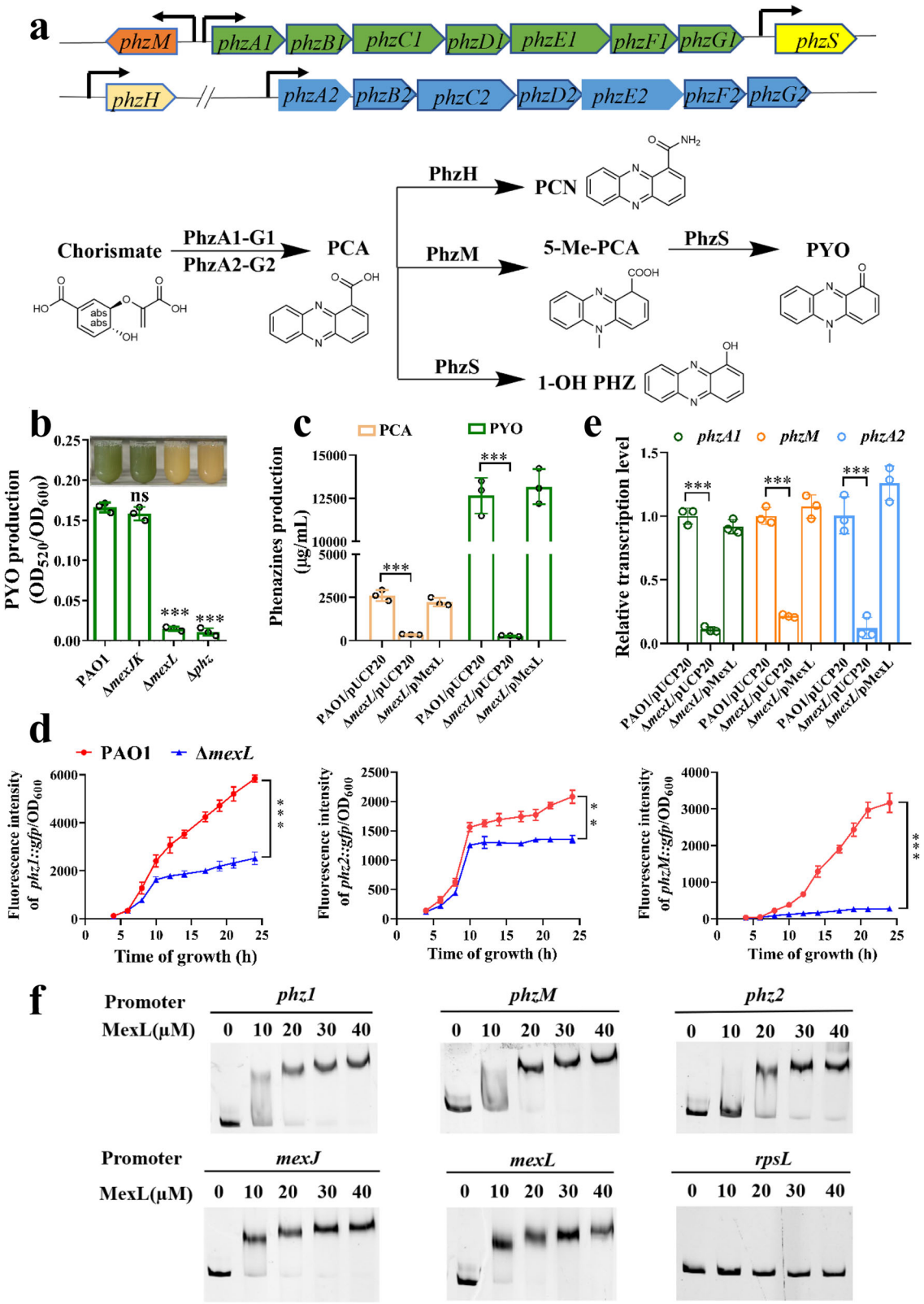

by degrading PYO[18]. These studies suggest that decreasing PYO production might be a potential way to control *P. aeruginosa* infections. However, it lacks an effective therapeutic target that can be utilized to reduce PYO production.

P. aeruginosa mainly produce four phenazines, including phenazine-1-carboxylic acid (PCA), phenazine-1-carboxamide (PCN), 1-hydroxyphenazine (1-OH-PHZ) and PYO. There are two gene clusters, *phzA1B1C1D1E1F1G1* and *phzA2B2C2D2E2F2G2* (referred as "*phz1*" and "*phz2*" in this study) responsible for the PCA biosynthesis. The conversion of PCA to PYO requires the enzymes encoded by *phzM* and *phzS*. PCA can also be catalyzed to PCN and 1-OH-PHZ via PhzH and PhzS, respectively (Fig. 1a)[19]. Many reports have indicated that phenazines biosynthesis is mainly controlled by the quorum sensing (QS) signaling system.

Fig. 1 | MexL was required for phenazine biosynthesis. a Phenazine biosynthesis pathway in *P. aeruginosa* PAO1. PCA, phenazine-1-carboxylic acid; PCN, phenazine-1-carboxamide; 5-Me-PCA, 5-methylphenazine-1-carboxylic acid; 1-OH-PHZ, 1-hydroxyphenazine; PYO, pyocyanin. PhzA1-G1 and PhzA2-G2, a series of proteins encoded by the *phzA1B1C1D1E1F1G1* and *phzA2B2C2D2E2F2G2* operons, respectively, plays role in the synthesis of PCA from chorismate; PhzH, PhzM and PhzS represent the key proteins during the synthesis of other phenazines by PCA, respectively. **b** PYO production of the PAO1, Δ*mexJK*, Δ*mexL* and Δ*phz* were determined after growth in LB medium for 16 h. ($n = 3$ independent experiments). **c** LC-MS/MS analysis of PCA and PYO production in PAO1, Δ*mexL* mutant, and the complemented strain in LB medium at 24 h post inoculation. ($n = 3$ independent experiments). **d** The promoter activity of *phz1*, *phz2* and *phzM* in PAO1 and Δ*mexL* reporter strains respectively post 24 h of growth. ($n = 3$ independent experiments). **e** RT-qPCR determination of the expression levels of *phzA1*, *phzA2* and *phzM* genes in PAO1, Δ*mexL* mutant, and the complemented strain. ($n = 3$ independent experiments). **f** Electrophoretic mobility shift assay (EMSA) revealed that MexL bound to the promoter *phz1*, *phz2* and *phzM*. The promoter regions of *mexL* and *mexJ* were used as the positive control, and the promoter region of 30S ribosomal S12 protein encoding gene *rpsL* was the negative control. Representative images were from three independent experiments. *P* values were determined using two-tailed Student's *t* test. Significance was indicated by a *P* value. ns, non-significant, $^{***}P < 0.001$, $^{**}P < 0.01$. **b** $P = 0.000334$ (PAO1 vs Δ*mexL*) and $P = 0.000112$ (PAO1 vs Δ*phz*). **c** $P = 0.000243$ (PCA) and $P = 0.000206$ (PYO). **d** $P = 0.000335$ (*phz1*), $P = 0.002031$ (*phz2*) and $P = 0.000171$ (*phzM*). **e** $P = 0.000238$ (*phzA1*), $P = 0.000384$ (*phzM*) and $P = 0.000794$ (*phzA2*).

Active efflux has critical contributions to the intrinsic resistance of *P. aeruginosa*[20]. The RND (Resistance-Nodulation-Cell Division) efflux system is the main efflux system in *P. aeruginosa* and at least 12 RND efflux pumps have been identified[21,22]. Growing evidence suggests the interplay between the efflux system and phenazines. PYO can protect *P. aeruginosa* from being killed by ciprofloxacin via transcriptional activation of two RND efflux pumps, MexGHI-OpmD and MexEF-OprN[8]. The MexGHI-OpmD was found to transport 5-methylphenazine-1-carboxylate (5-Me-PCA), a type of phenazines and the precursor for PYO synthesis[23]. The redox-sensing transcription factor SoxR indirectly activates the expression of MexGHI−OpmD efflux system in response to PYO[8,15]. However, the mechanisms by which the efflux systems affect phenazines remain largely unclear.

A typical RND efflux pump is a tripartite protein complex, consisting of an inner membrane protein, a membrane fusion protein and an outer membrane protein channel[24]. The MexJK-OprM efflux pump consists of the inner membrane protein MexK, the membrane fusion protein MexJ, and the outer membrane protein OprM, which is shared with several other efflux systems, including MexAB, MexMN, MexVW, and MexXY[25]. The MexJK-OprM efflux pump has a relatively narrow substrate spectrum, by which two antibiotics, tetracycline (TET) and erythromycin (ERY) have been identified for effluxion[25]. In addition, MexJK can also extrude triclosan (TCS) by associating with the outer membrane protein OpmH[26]. Recent research has proposed that the MexJK efflux could modulate QS response[27]. The expression of MexJK-OprM efflux pump is upregulated in an ex vivo pig model of the cystic fibrosis lung, suggesting that this efflux pump may play a role in chronic infection caused by *P. aeruginosa*[28]. The expression of *mexJK* was repressed by a transcriptional regulator MexL, which was encoded by *mexL* located upstream of *mexJK* operon in the opposite direction[29].

In this work, we show that MexL, the repressor of *mexJK*, directly activates the phenazine biosynthesis in *P. aeruginosa*, and PYO can autoregulate its own production by affecting the activity of MexL. The *mexL* knockout mutant has significant reduction in virulence and pathogenesis, suggesting its potential as a therapeutic target. Further investigations have suggested a role of several antimicrobials in reducing the virulence of *P. aeruginosa* by interfering with MexL. We have also provided antibiotic combinations to combat *P. aeruginosa* infections in a murine acute pneumonia animal model. Our findings prove the concept that targeting virulence can be an effective way of antimicrobial therapy.

Results

The multidrug efflux pump repressor MexL directly activates the biosynthesis of phenazines

In an investigation on whether the MexJK-OprM efflux pump is involved in phenazines secretion, we constructed two in-frame deletion mutants in *P. aeruginosa* PAO1 strain, Δ*mexJK* and Δ*mexL*. In agreement with the previous publication depicting MexL as a transcriptional repressor[27], the transcription of *mexJK* in the Δ*mexL* background was higher than that of PAO1 (Figure S1a and S1b), while deletion of *mexJK* or *mexL* did not affect bacterial growth or biofilm formation (Figure S1c and S1d). Unexpectedly, phenazines production of Δ*mexL* and Δ*mexJK* had remarkable differences. The Δ*mexJK* strain produced similar amount of PYO and PCA as that of PAO1 (Fig. 1b and Figure S1e), suggesting that the MexJK efflux is unlikely involved in phenazines secretion. In contrast, the phenazines production of Δ*mexL* was as low as the phenazine biosynthesis-abolished mutant Δ*phz* (in which the two key gene clusters *phz1* and *phz2* were deleted) (Fig. 1b and Figure S1e). This result is consistent with the report of Amieva et al. [27], in which the PYO reduction was proposed to be a result of QS defect. The expression of MexL in the Δ*mexL* mutant restored phenazine biosynthesis to the wild-type level (Fig. 1c), confirming that MexL did affect phenazine production.

To understand how MexL affects phenazine biosynthesis, we first detected the transcriptional level of genes involved in phenazine biosynthesis (Fig. 1a), namely *phz1*, *phz2*, *phzH*, *phzM*, and *phzS*, in Δ*mexL* and wild type strain PAO1 respectively by using the promoter-*gfp* fusion reporter plasmids. Compared to PAO1, Δ*mexL* significantly decreased the transcription of *phz1*, *phz2* and *phzM* (Fig. 1d), while showing no effect on *phzH* and *phzS* expression (Figure S1f). The reduced transcription of *phzA1*, *phzA2*, and *phzM* in Δ*mexL* was further confirmed by RT-qPCR analysis, and the transcriptional reduction of these genes can be restored by complementation with the *mexL* in trans (Fig. 1e). These results indicated that the MexL affected phenazine production by activating the transcription of *phzM* and the gene clusters *of phz1 and phz2*.

To further determine whether MexL can directly bind the promoters of *phz1*, *phz2*, and *phzM* to regulate phenazine biosynthesis, we conducted the electrophoretic mobility shift assay (EMSA). In this assay, the promoters of *mexL* and *mexJ* were used as positive controls, and the promoter of *rpsL* (encoding 30S ribosomal protein) was served as a negative control. EMSA results showed that MexL was efficiently bound to the promoter regions of *phz1*, *phzM* and *phz2* respectively in a dose-dependent manner (Fig. 1f). Taken together, our data showed that the efflux pump repressor MexL could function as a transcriptional activator to enhance the expression of several phenazine biosynthesis genes and thus increase the phenazine production.

Identification of the conserved MexL-binding DNA motif reveals the mechanism for how MexL functions as a repressor and an activator

To determine the MexL-binding motif in the promoters of *mexJ*, *phz1*, *phzM*, and *phz2*, a series of truncations was designed on the corresponding promoter region and their MexL-binding capabilities were tested by EMSA. As shown in Fig. 2a, the shortest MexL-binding regions were nailed within 122 bp upstream of the ATG start codon of *mexJ* (-122 bp), from -250 bp to -135 bp in the *phz1* promoter, -256 bp to -203 bp in the *phzM* promoter, and in a 104 bp region from -296 bp to -193 bp in the *phz2* promoter respectively (Fig. 2a). Based on these binding regions, we utilized MEME online tool to analyze the possible conserved DNA motifs that MexL may bind to. It revealed a consensus

https://doi.org/10.1038/s41467-025-57294-8

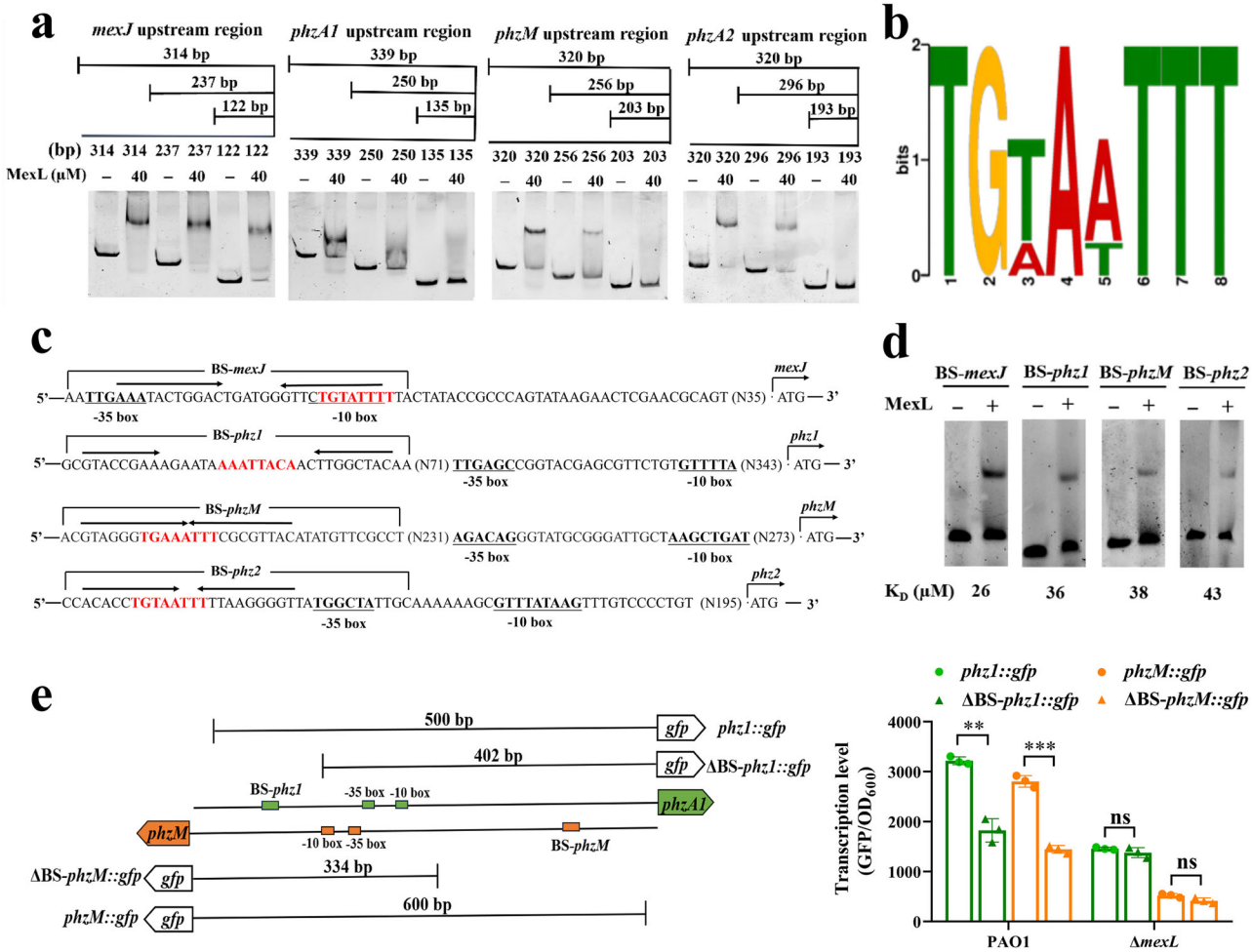

Fig. 2 | Identification of the conserved MexL-binding motif within promoters. **a** Determination of binding ability of MexL with truncated *mexJ*, *phz1*, *phz2* and *phzM* promoter region by EMSA, respectively. Representative images from three independent experiments. **b** The predicted MexL-binding consensus motif (5′-TGTAATTT-3′) obtained by MEME online tools. **c** Sequence of the *mexJ*, *phz1*, *phz2* and *phzM* promoter regions carrying potential MexL binding site. The predicted MexL binding site were shown in red letter, and the location of palindromes in each promoter region was marked by inverted arrows. **d** Four binding site (BS-*mexJ*, BS-*phz1*, BS-*phzM* and BS-*phz2*) were tested by EMSAs. Microscale thermophoresis (MST) analysis the binding affinities of MexL to BS-*mexJ*, BS-*phz1*, BS-*phz2* and BS-*phzM* promoter, respectively, and the corresponding K_D (dissociation constant) value was shown under the image. Representative images were from three independent experiments. **e** Confirming the MexL-binding sites in *phz1* and *phzM* promoters. The left panel is the schematic diagrams of the *phz1* and *phzM* promoter regions and corresponding promoter::*gfp* fusion reporter plasmids. ΔBS-*phz1::gfp* indicates the *phz1::gfp* reporter without the BS-*phz1* site. ΔBS-*phzM::gfp* is *phzM::gfp* reporter without the BS-*phzM* site. The column at the right is the fluorescence intensity of corresponding promoter::*gfp* fusion reporter plasmid in PAO1 and Δ*mexL* strains post 24 h of growth. ($n = 3$ independent experiments). *P* values were determined using two-tailed Student's *t* test. Significance was indicated by a *P* value. ns, non-significant, $^{***}P < 0.001$, $^{**}P < 0.01$. **e** $P = 0.001528$ (PAO1/*phz1::gfp* vs PAO1/ΔBS-*phz1::gfp*), $P = 0.000198$ (PAO1/*phzM::gfp* vs PAO1/ΔBS-*phzM::gfp*).

motif of 5′-TGTAATTT-3′ or its complementary 5′-AAATTACA-3′ (Fig. 2b). The TetR family transcriptional regulators usually bind to DNA as a homodimer and recognize a palindromic sequence. The palindromic sequences containing the consensus MexL-binding motif were found in the promoters of the above four MexL-regulated genes (Fig. 2c). To further confirm, we synthesized these four corresponding DNA regions, namely BS-*mexJ*, BS-*phz1*, BS-*phzM*, and BS-*phz2*, respectively, each of which includes the conserved MexL-binding DNA motifs and the corresponding palindromic sequences (Fig. 2c). EMSA analysis showed that all the four DNA regions could interact with MexL (Fig. 2d). Interestingly, the consensus MexL-binding motif is located on the TATA box in the promoter of *mexJ* (Fig. 2c), in which MexL functions as a repressor. However, as for *phz1*, *phzM*, and *phz2*, in which MexL serves as an activator, the MexL-binding motif is upstream of the TATA box (Fig. 2c). These results suggest that MexL functioning as an activator or repressor is mainly depended on its binding location within the promoters. We then further quantified the binding affinities of MexL for the promoters of above four genes using MST analysis. The dissociation constants (K_D) of MexL with the promoters of *phz1*, *phzM*, and *phz2* was proximately 1.5-fold higher than that for *mexJ* (K_D is 26 μM), suggesting a stronger binding affinity of MexL to the promoter of *mexJ*, which was consistent with the EMSA results (Fig. 2d). To further confirm the MexL-binding site of *phzA1* and *phzM* respectively, we constructed the corresponding ΔBS-*phz1::gfp* and ΔBS-*phzM::gfp* reporter plasmids (where ΔBS indicates the deletion of the binding site) (Fig.2e, left panel). As shown in Fig.2e, removal of the corresponding MexL-binding site from the tested promoter regions significantly reduced the expression of *phz1* and *phzM* in PAO1, but had little effect on the transcription of either *phz1* or *phzM* in Δ*mexL* mutant. These results further confirmed that the effect of MexL on the transcription of *phz1 and phzM* required in the presence of both MexL and its corresponding binding sites.

Crystal structure of MexL and the key amino acids for DNA-binding

The apo-form crystal structure of $MexL_{15\text{-}212}$ was determined in the space group $P3_221$ at a resolution of ~3.0 Å. Only one dimeric model of

Table 1 | Data collection and refinement statistics of $MexL_{15-212}$

	$MexL_{15-212}$ (PDB: 8WRF)
Date collection*	
Space group Unit-cell	$P3_221$
a,b,c (Å)	103.09, 103.09, 146.64
α/β/γ (°)	90, 90, 120
Resolution (Å)	30.65-3.0 (3.11-3.0)
Unique reflections	18558 (1815)
Redundancy	19.3 (20.7)
Completeness (%)	99.84 (100.00)
I/σ(I)	43.86 (12.49)
R_{merge}	0.057 (0.289)
$CC_{1/2}$	1 (0.992)
Refinement	
R_{work}/R_{free}	0.210/0.243
No. atoms	
Protein	3074
Ligands	/
B-factor (Å^2)	
Protein	77.51
Ligands	/
R.m.s deviations	
Bond length (Å)	0.010
Bond angles (°)	1.18
Ramachandran Plot	
Favored (%)	94.67
Allowed (%)	4.57
Outliers (%)	0.76

*Values in parentheses refer to the highest resolution shell.

$MexL_{15-212}$ was successfully built into the electron density within an asymmetric unit (Table 1). The overall architecture of $MexL_{15-212}$ is consistent with the structures of other TetR family transcriptional regulators (Fig. 3a). The two subunits of $MexL_{15-212}$ are very similar in structure with a root mean square deviation (RMSD) around 0.946 Å (between Cα atoms). $MexL_{15-212}$ is composed of a DNA-binding domain at the N-terminus (NTD, helices α1 to α3) and a ligand-binding domain at the C-terminus (CTD, helices α4 to α10), which are linked by a hinge region. The helices α2 and α3 of NTD form a typical helix-turn-helix (HTH) motif accounting for recognition and binding of the target DNA. The helices 6, 8, 9 and 10 of CTD comprise the dimerization interface (~1545 Å^2).

To dissect regulation mechanism of MexL, the MexL structure was examined and compared to its TetR homologs with highest structural similarities. The top three TetR-family transcriptional regulators with similar structures to $MexL_{15-212}$ were identified using the DALI server[30], which including FrrA (PDB: 6G87, RMSD ~ 3.33 Å) from *Bradyrhizobium diazoefficiens*[31], FadR (PDB: 5GPA, RMSD ~ 3.52 Å) from *Bacillus halodurans*[32] and QacR (PDB: 2HQ5, RMSD ~ 5.06 Å) from *Staphylococcus aureus*[33]. These structures diverge most within the ligand binding domains, and the ligand binding modes of FrrA, FadR and QacR are quite different. Both $MexL_{15-212}$ and FrrA contain seven α helices in the C-terminal ligand-binding domain, in contrast to only six α helices in CTD of most other TetR family regulators.

The MexL DNA-binding domain was superposed onto the FadR-DNA (PDB:5GPC)[32] and QacR-DNA (PDB: 1JT0)[34] complex structures to investigate the possible DNA recognition mode of MexL (Figure S2). These proteins bind to DNA mainly by inserting the helix α3 of NTD in the major groove. The conserved residues likely involved in DNA interactions were identified (labeled with asterisk in Figure S2). Multiple amino acid sequence alignment of the DNA-binding domains of MexL and other TetR family proteins was further performed, indicating that the 47th alanine (47 A), the 48th glycine (48 G) and 55th tyrosine (55Y) residues within the HTH DNA-binding domain were highly conserved within the TetR family (Fig. 3b). Previous data have shown that the A47D mutation prevents the binding of MexL from the *mexJ* promoter[29]. By generating a structure model of the MexL A47D mutant using the AlphaFold2[35], we found that D47 could form hydrogen bond with R29 of helix 1, the interaction of which doesn't exist in the structure of the wild type MexL (Fig. 3c). This D47-R29 interaction may greatly restrict the movement of helices 2 and 3 that is required for accommodating DNA binding. In fact, it was proven that the A47D mutation in MexL did result in loss of its binding ability to the promoter regions of *mexJ*, *phz1*, *phz2*, and *phzM* in vitro (Fig. 3d). Complementing the *mexL* deletion strain with MexL(A47D) also failed to restore the pyocyanin production and the transcription levels of *phzA1*, *phzA2* and *phzM* genes (Fig. 3e and f), suggesting that MexL interacts with all these promoters in a similar mode and the residue A47 plays an important role in the MexL-DNA interaction.

Feedback regulation of pyocyanin on its own production through MexL

Antibiotics often act as a ligand of their regulators, thus we further investigated whether PYO could function as a ligand of MexL. We first performed a molecular docking analysis by using the C-terminal ligand-binding domain of a protomer of $MexL_{15-212}$, which resulted in a docking score of -6.8 kcal/mol (Fig. 4a). This score falls within the range of known antibiotic ligands (the docking scores are from −6.7 to −9.0 kcal/mol)[36], suggesting that PYO can be a ligand of MexL. We then examined the PYO-MexL interaction in vitro. The thermal stability of MexL with/without PYO or PCA was measured by using a method based on the label-free nanoDSF. In the presence of 250 μM PYO, MexL showed a detectable decrease in melting temperature (T_m) from 61.8 to 57.7 °C, whereas PCA had no significant effect on MexL (Fig. 4b, left panel). In addition, the T_m of MexL gradually decreased as the concentration of PYO increased (Fig. 4b, middle panel). The binding affinity constant (K_D) between PYO and MexL was determined by the BioLayer interferometry (BLI) with a K_D value of 84.2 ± 1.8 μM, (Fig. 4b, right panel). To investigate the effect of PYO or PCA on the MexL-DNA interaction, we added different concentrations of PYO or PCA in the EMSA reactions. PYO dissociated MexL from the promoter of *phz1*, *phz2*, *phzM* or *mexJ* in a dose dependent manner (Fig. 4c). However, the addition of PCA did not show any effect on the MexL-promoter interaction (Fig. 4c). The MST analysis showed that the addition of PYO doubled the K_D value of the MexL-DNA interaction (Fig. 4d), indicating a decrease in the DNA-binding affinity of MexL in the presence of PYO. These data show that PYO can interact with MexL in vitro and the PYO-MexL interaction interferes the DNA binding activity of MexL.

We then examined the effect of supplementing PYO in the culture of either PAO1 or Δ*mexL* mutant. In consistent with the in vitro data, addition of 500 μM PYO in PAO1 culture decreased the expression of *phz1*, *phzM*, and *phz2* by 50%, and the transcription of *mexJ* in PAO1was increased at a PYO dose dependent manner. In contrast, addition of PYO had no effect on the expression of these genes in Δ*mexL* mutant (Fig. 4e and f). These results indicate that the effect of PYO on the transcription of these genes is MexL-dependent. In addition, based on the docking result, we mutated two key amino acid residues (F169 and K173) in the predicted PYO binding pocket of MexL. Both of the MexL variants, MexL(F169A) and MexL(K173A), lost DNA binding ability and were unable to recover the PYO production in Δ*mexL* background (Figure S2c), which confirmed the PYO binding pocket in MexL and suggested how PYO might affect the DNA-binding of MexL.

Taken together, our data suggest that PYO acts as a ligand of MexL to trigger a conformational rearrangement of this regulator that consequently affects its DNA binding capability, leading to changes in the

https://doi.org/10.1038/s41467-025-57294-8

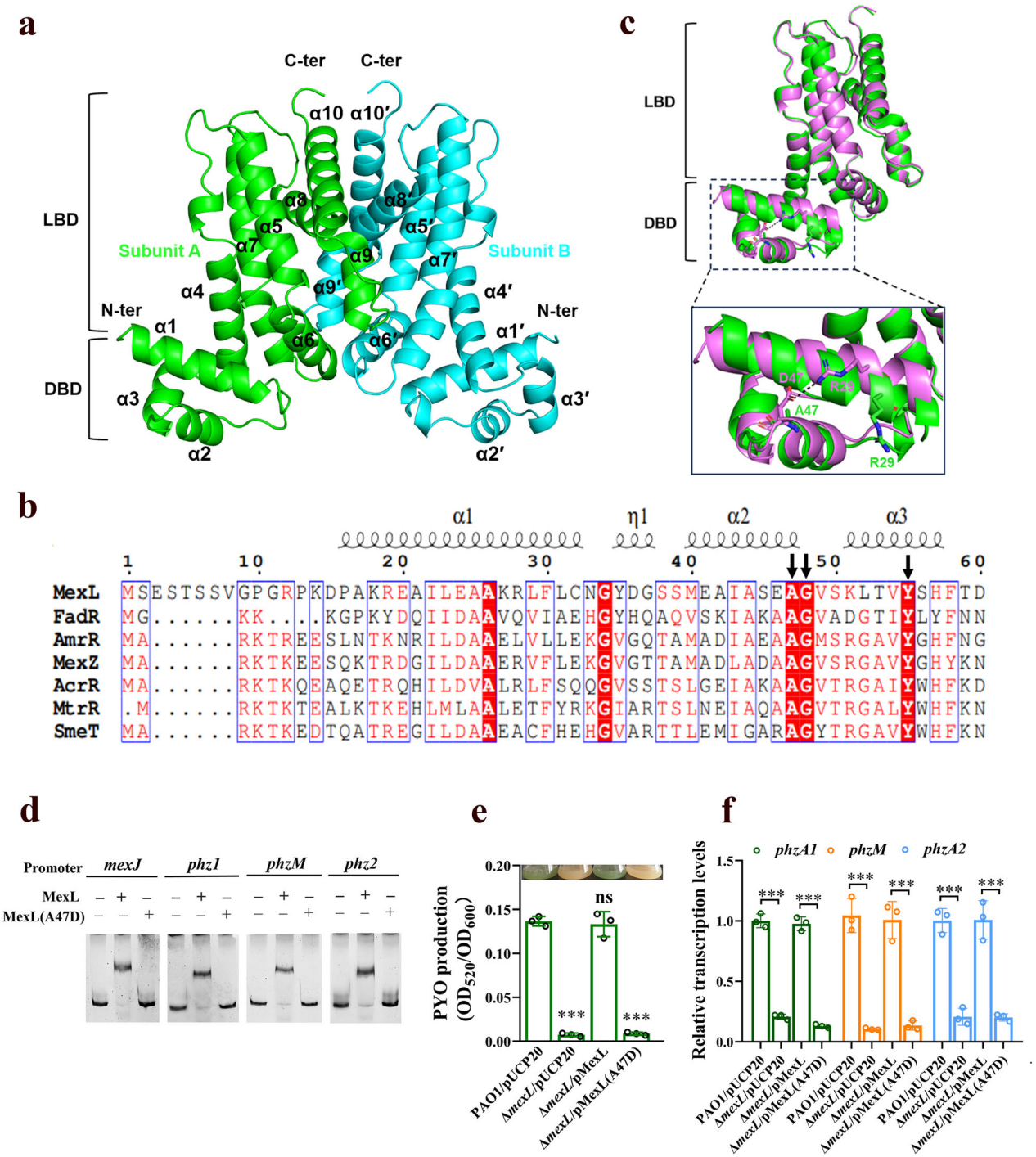

Fig. 3 | Crystal structure of MexL$_{15\text{-}212}$ and the key amino acids for DNA-binding. **a** Ribbon diagram of the MexL$_{15\text{-}212}$ dimer. Subunit A was shown in green; subunit B was shown in cyans. LBD, ligand-binding domain in C-terminus, consist of seven α helices, α4 to α10. DBD, the N-terminal DNA-binding domain is composed of three helices, α1 to α3. **b** The alanine (A) of 47, glycine (G) of 48 and tyrosine (Y) of 55 in MexL was highly conserved in TetR family regulator. Shown was the multiple sequence alignment of the HTH DNA-binding domain of MexL and other TetR family regulator, including FadR from *Bacillus halodurans*, MexZ of *P. aeruginosa*, MtrR of *Neisseria gonorrhoeae*, AcrR of *Escherichia coli*, AmrR of *Burkholderia pseudomallei* and SmeT of *Stenotrophomonas maltophilia*. **c** Structure alignment between MexL and MexL(A47D). MexL and MexL(A47D) are shown in green and magenta, respectively. The hydrogen bond interaction between D47 and R29 is shown as black dashed lines. **d** Electrophoretic mobility shift assay (EMSA) detection of binding of MexL and MexL(A47D) to the *mexJ*, *phz1*, *phz2* and *phzM* promoter, respectively. Representative images from three independent experiments. **e** PYO production of the PAO1/pUCP20, Δ*mexL*/pUCP20, Δ*mexL*/pMexL and Δ*mexL*/pMexL (A47D) were measured after culture in LB medium for 16 h. ($n = 3$ independent experiments). **f** RT-qPCR determination of the expression levels of *phzA1*, *phzA2* and *phzM* genes in the PAO1/pUCP20, Δ*mexL*/pUCP20, Δ*mexL*/pMexL and Δ*mexL*/pMexL (A47D). ($n = 3$ independent experiments). *P* values were determined using two-tailed Student's *t* test. Significance was indicated by a *P* value. ns, non-significant, $^{***}P < 0.001$. **e** $P = 0.000945$ (PAO1/pUCP20 vs Δ*mexL*/pUCP20), $P = 0.000792$ (PAO1/pUCP20 vs Δ*mexL*/pMexL(A47D)). **f** $P = 0.000161$(PAO1/pUCP20 vs Δ*mexL*/pUCP20 (*phzA1*)), $P = 0.00015$ (Δ*mexL*/pMexL vs Δ*mexL*/pMexL(A47D) (*phzA1*)), $P = 0.000328$ (PAO1/pUCP20 vs Δ*mexL*/pUCP20 (*phzM*)), $P = 0.00063$ (Δ*mexL*/pMexL vs Δ*mexL*/pMexL(A47D) (*phzM*)), $P = 0.000349$ (PAO1/pUCP20 vs Δ*mexL*/pUCP20 (*phzA2*)) and $P = 0.000981$ (Δ*mexL*/pMexL vs Δ*mexL*/pMexL(A47D) (*phzA2*)).

https://doi.org/10.1038/s41467-025-57294-8

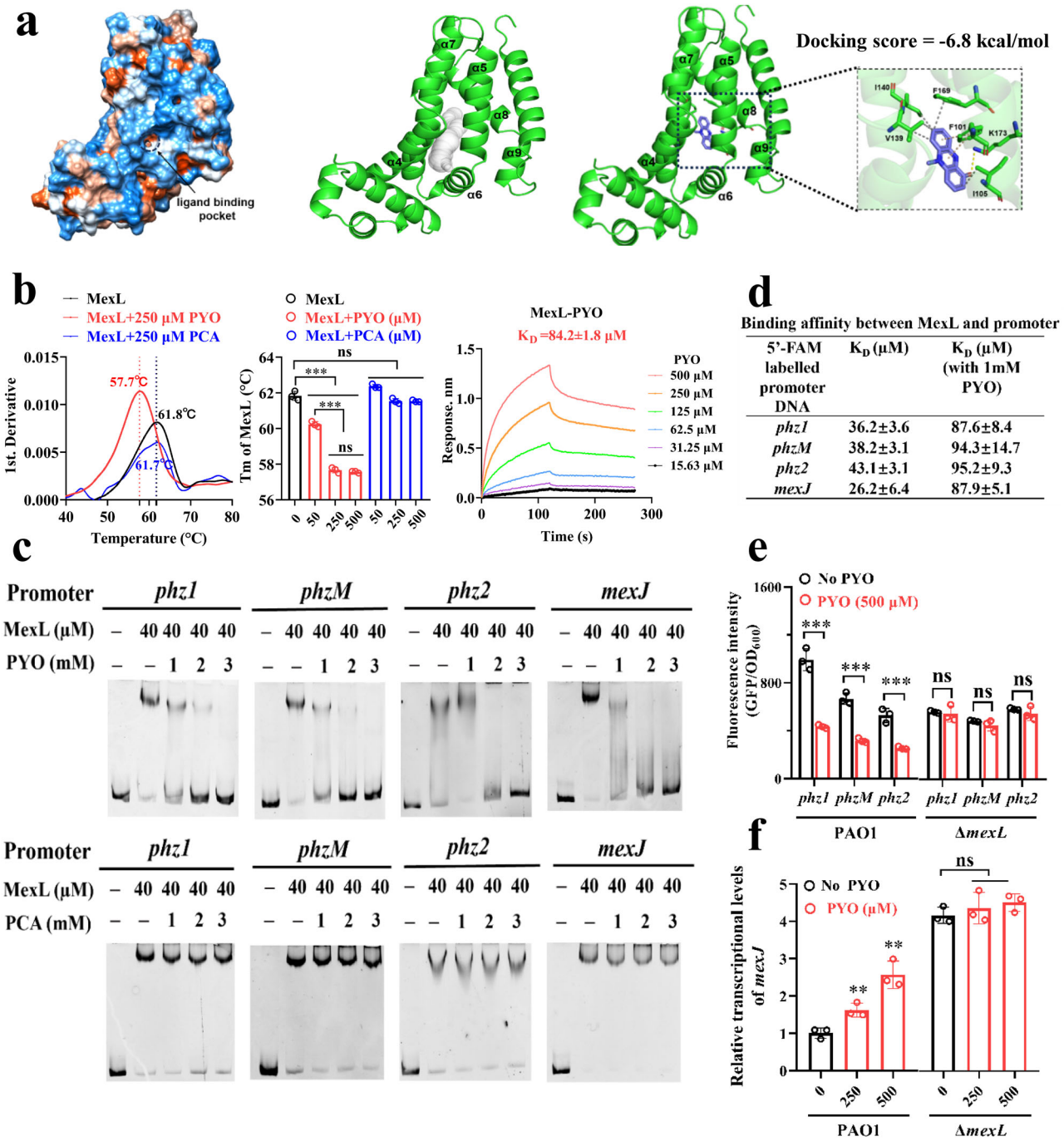

Fig. 4 | Feedback regulation of pyocyanin on its own production through MexL. **a** Docking of PYO to the structure of $MexL_{15\text{-}212}$. Left, hydrophobic surface of subunit A of $MexL_{15\text{-}212}$, blue represents hydrophilic surface, orange represents hydrophobic surface. Middle, ribbon diagram of subunit A of $MexL_{15\text{-}212}$. The ligand substrate tunnel shown in gray. Right, the interaction between $MexL_{15\text{-}212}$ and PYO. **b** Detection of the interaction between MexL and PYO in vitro. **Left panel**, thermal-shift analyzes the purified MexL bound to PYO and PCA. The MexL sample were incubated with DMSO (no phenazines), 250 μM PYO (red trace), 250 μM PCA (blue trace), respectively. **Middle panel**, the corresponding Tm of MexL in the presence of different concentrations of PYO and PCA, respectively. **Right panel**, Octet Red 96 determine the binding affinity (K_D) between MexL and PYO. The K_D value was 84.2 ± 1.8 μM. ($n = 3$ independent experiments). **c** EMSA analysis the interaction between MexL and promoter in the presence of PYO and PCA, respectively. Representative images were from three independent experiments. **d** Microscale thermophoresis (MST) analysis the binding affinities of MexL to *mexJ*, *phz1*, *phz2* and *phzM* promoter in the presence or absence of 1 mM PYO, respectively. K_D was the dissociation constant. ($n = 3$ independent experiments). **e** Analysis of promoter activity of *phz1*, *phz2* and *phzM* in PAO1 and Δ*mexL* by corresponding promoter::*gfp* reporter plasmids in the presence of 500 μM PYO. ($n = 3$ independent experiments). **f** RT-qPCR determine the transcriptional level of *mexJ* in the presence of PYO. ($n = 3$ independent experiments). *P* values were determined using two-tailed Student's *t* test. Significance was indicated by a *P* value. ns, non-significant, $^{***}P < 0.001$, $^{**}P < 0.01$. **b** $P = 0.00071$ (0 μM vs 50 μM), 0.000152 (0 μM vs 250 μM), 0.000168 (0 μM vs 500 μM), 0.000732 (50 μM vs 250 μM) and 0.000659 (50 μM vs 500 μM). **e** $P = 0.000464$ (*phz1*), 0.000326 (*phzM*) and 0.000625 (*phz2*). **f** $P = 0.009945$ (0 μM vs 250 μM) and 0.0023 (0 μM vs 500 μM).

https://doi.org/10.1038/s41467-025-57294-8

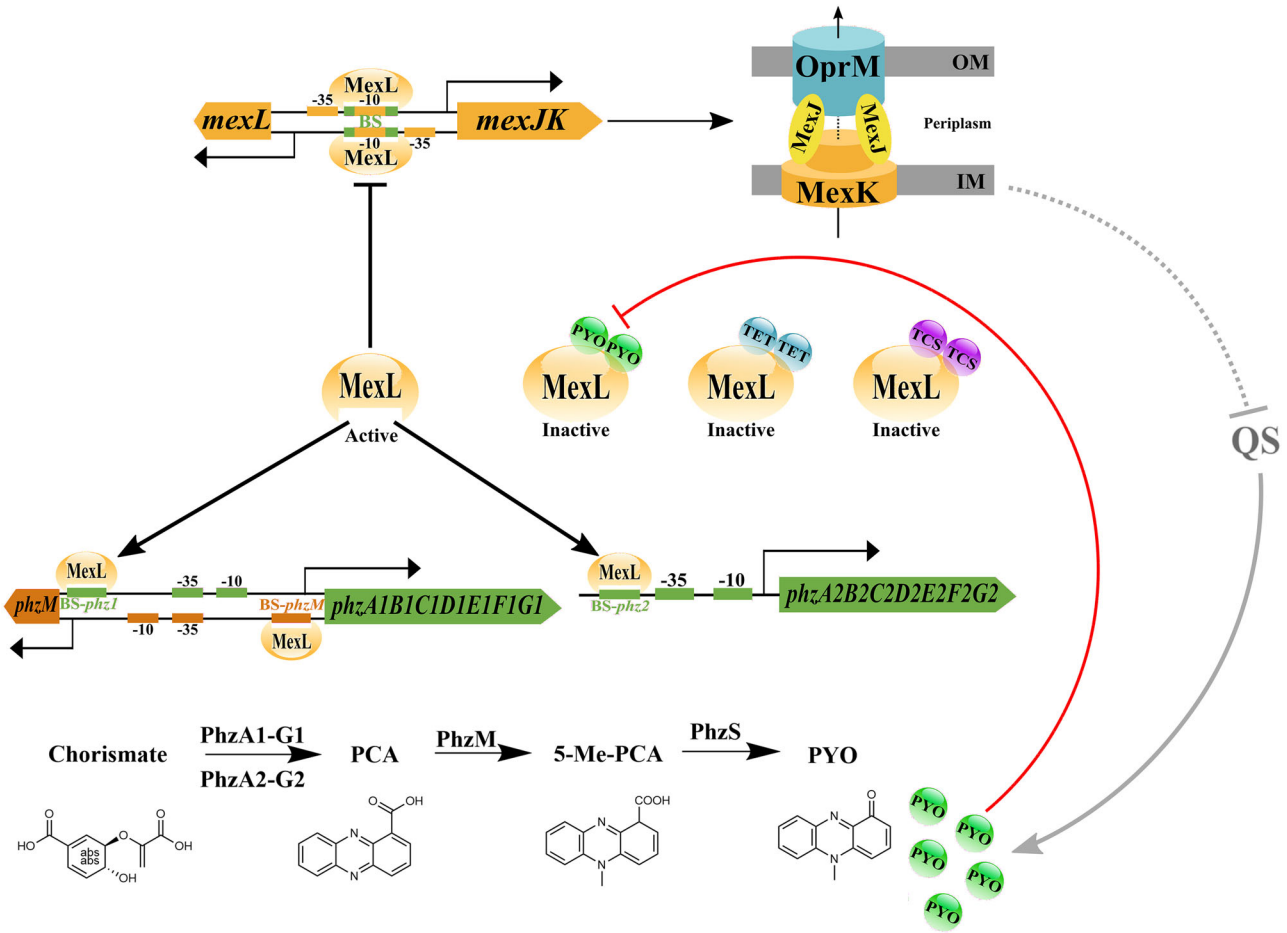

Fig. 5 | The mechanism of interplay between the MexJK-OprM efflux pump and the phenazine synthesis. A schematic diagram to show a MexL-mediated cross regulation between the MexJK-OprM efflux pump and the phenazine synthesis. MexL represses the MexJK-OprM efflux pump and its own expression and binds to the promoter regions of *phz1*, *phz2* and *phzM* to activate phenazine synthesis. Low level PYO allows MexL to activate phenazine synthesis and meanwhile to repress the expression of MexJK. When PYO reach a higher level (> 50 μM), it interferes the DNA-binding activity of MexL, thus reduces phenazine synthesis and meanwhile allow the expression of MexJK. TET and TCS, both compete with PYO to interact with MexL, thus inactivate MexL and decrease PYO production. As previous reported[26] that the overexpression of MexJK can inhibit quorum sensing (QS) signaling, thereby reducing PYO production. OM: outer membrane; IM: inner membrane. Solid black line with arrow: activation, solid black line with bar: repression, solid red line with bar: PYO negatively feedback regulates its own synthesis by interfering with MexL binding to the promoters. BS: the binding site of MexL on the *mexJ*, *phz1*, *phz2* and *phzM* promoter, which contains consensus motif (5′-TGTAATTT-3′) or the complementary sequence (5′-AAATTACA-3′).

expression of the MexL-regulated genes. These results also indicate that PYO serves as a terminal signal to regulate its own synthesis through a negative feedback loop (Fig. 5).

The antimicrobials interfering with the function of MexL can reduce PYO production and the virulence of *P. aeruginosa*

As PYO is an important virulent factor of *P. aeruginosa* and *mexL* knockout remarkably decreases PYO production as shown above, we propose that MexL can be utilized as a therapeutic target to reduce PYO production and virulence. In support of this, Δ*mexL* mutant did show less virulence than PAO1 on human alveolar epithelial cells A549 and less toxicity to *Staphylococcus aureus* (Figure S3). We then searched for other possible ligands of MexL by selecting compounds with a chemical structure similar to PYO, and that can be extruded out by the MexJK efflux pump. This led to two antimicrobials, tetracycline (TET) and triclosan (TCS). The docking analysis suggested that PYO, TET and TCS, all were fit in the same pocket within the C-terminal ligand-binding domain of MexL (Fig. 6a). Similar to the observed effect of PYO, both TET and TCS also significantly reduce the Tm values of MexL (Fig. 6b), indicating their interaction with MexL. In addition, these two antimicrobials both can interfere with the DNA-binding activity of MexL in EMSA, while Tobramycin (TOB) did not show such an effect (Figure S4a). This result was in agreement with their effect on the expression of *mexJ*. As shown in Figure S4b, TET and TCS both increased the expression of *mexJ*, yet TOB showed no effect on the *mexJ*'s expression. These data suggest that PYO, TET and TCS compete in binding with MexL. We then checked the effect of TET or TCS at the sub-inhibitory concentration on the PYO production. With no significant effect on bacterial growth, TET and TCS both decreased the expression of phenazine synthesis genes and dramatically inhibited the PYO production in PAO1 (Fig. 6c and d). We next examined whether TET or TCS treatment can reduce the virulence of *P. aeruginosa*. The PAO1 strain was treated with TET or TCS at sub-inhibitory concentrations for overnight, and then was used to infect A549 cells respectively. The cells infected by either the Δ*mexL* mutant, TET or TCS-pretreated PAO1, or Δ*phz* mutant, all exhibited higher cell viability compared to those infected with PAO1 without pre-treatment, indicating that TET or TCS pre-treated PAO1 was less virulent (Fig. 6e). We also tested the cytotoxicity of TET or TCS-pretreated Δ*mexL* strains. The A549 cell viability had no significant difference when infected by Δ*mexL* with or without TET or TCS pretreatment, suggesting that TET or TCS might reduce the virulence of PAO1 by acting on MexL (Fig. 6e). To rule out

https://doi.org/10.1038/s41467-025-57294-8

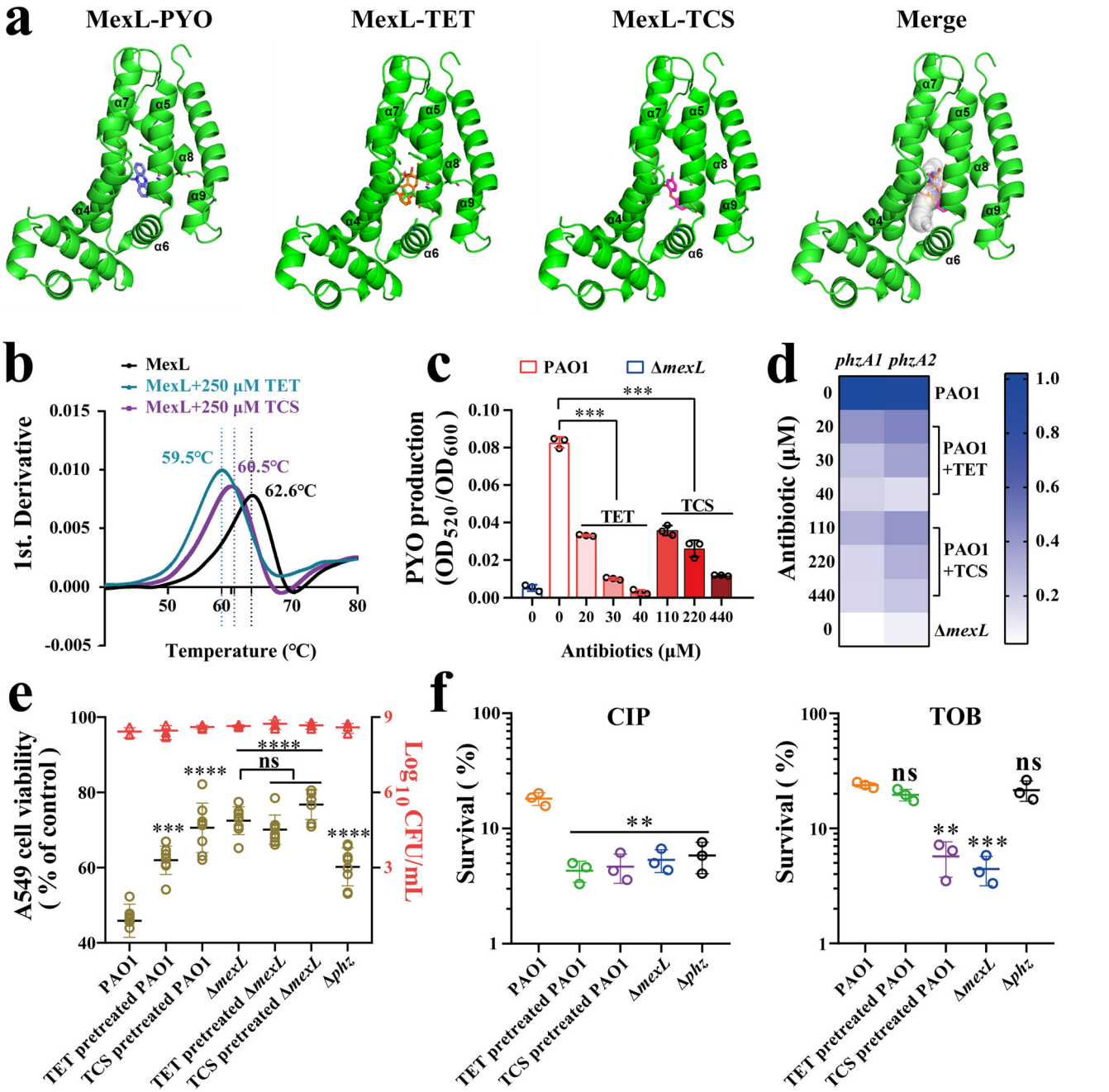

Fig. 6 | The effect of TET or TCS on the activity of MexL and the virulence of *P. aeruginosa*. **a** Docking of PYO, TET and TCS to the structure of $MexL_{15\text{-}212}$, respectively. The docking substrates located in the tunnel shown in stick model are PYO (slate), TET (orange) and TCS (magenta). **b** Thermal-shift analyzes MexL interactions with TET and TCS, respectively. ($n = 3$ independent experiments). **c** Sub-inhibitory concentrations of TET or TCS can reduce PYO production of PAO1 to a level close to Δ*mexL*. ($n = 3$ independent experiments). **d** Heat map showing differential expression patterns of *phzA1* and *phzA2* genes in the presence of sub-inhibitory concentrations of TET and TCS. Data were obtained by RT-qPCR analysis, and expression level of *phzA1* and *phzA2* in PAO1 was regarded as 1. ($n = 3$ independent experiments). **e** The cell viability of A549 lung epithelial cell detected by the CCK-8 assay post *P. aeruginosa* infection. Shown in red is the CFU of these strains that were used to infect A549 cells. ($n = 8$ independent experiments). **f** The effect of TET and TCS on the antibiotic tolerance of PAO1. The survival rate was measured post 4 h treatment of ciprofloxacin (CIP, 1 μg/mL) or tobramycin (TOB, 4 μg/mL). ($n = 3$ independent experiments). *P* values were determined using two-tailed Student's *t* test. Significance was indicated by a *P* value. ns, non-significant, $^{****}P < 0.0001$, $^{***}P < 0.001$, $^{**}P < 0.01$. **c** $P = 0.000197$ (0 vs 20 μM TET), 0.000102 (0 vs 30 μM TET), 0.000122 (0 vs 40 μM TET), 0.000178 (0 vs 110 μM TCS), 0.00015 (0 vs 220 μM TCS) and 0.000138 (0 vs 330 μM TCS). **e** $P = 0.000151$ (PAO1 vs TET pretreated PAO1), 4.2E-07 (PAO1 vs TCS pretreated PAO1), 3.57E-10 (PAO1 vs Δ*mexL*), 1.37E-08 (PAO1 vs TET pretreated Δ*mexL*), 1.25E-09 (PAO1 vs TCS pretreated Δ*mexL*) and 3.07E-05 (PAO1 vs Δ*phz*). **f** $P = 0.001031$ (PAO1 vs TET pretreated PAO1, CIP), 0.001491 (PAO1 vs TCS pretreated PAO1, CIP), 0.001328 (PAO1 vs Δ*mexL*, CIP), 0.001494 (PAO1 vs Δ*phz*, CIP), 0.00107 (PAO1 vs TCS pretreated PAO1, TOB) and 0.000123 (PAO1 vs Δ*mexL*, TOB).

the possibility that the TET or TCS-pretreatment might decrease the total protein level of PAO1, we measured the amount of total protein of PAO1 undergoing post-overnight treatment with TET or TCS, meanwhile detecting the protein level of MexL with the anti-MexL antibody. Compared to PAO1 without treatment, the TET or TCS treatment at sub-inhibitory concentration did not alter the total protein level and the amount of MexL in PAO1 (Figure S5a). This was consistent with the fact that little effect was found for TET or TCS treatment on PAO1 and

the Δ*mexL* strain, regarding to growth and swarming motility (Figure S5b and c).

We further assessed the pathogenicity of PAO1, the Δ*mexL* mutant, and PAO1 pretreated with TET at sub-inhibitory concentration in a murine acute pneumonia model by intranasal infection on mice. Infections with all strains were sublethal with an intranasal challenge inoculum of 2×10^6 CFU (colony-forming units). Infections with PAO1 resulted in the most severe weight loss in mice at 1 dpi (day post-infection) although bacterial loads in the lungs of three infected groups were similar (~10^3 CFU) (Figure S6). Histological examination of the lung lobes showed intense inflammatory infiltration in the PAO1-infected group from 1 to 6 dpi. Notably, little inflammatory infiltration was found for the Δ*mexL* mutant or TET-pretreated PAO1 infection groups (Figure S6). These results have suggested that the Δ*mexL* mutant and TET-pretreated PAO1 trigger less inflammatory responses and thus reduce the damage in lung tissue compared to untreated PAO1 strain. Taken together, our data suggest that TET and TCS can be used for reducing the virulence of *P. aeruginosa*.

TET or TCS-pretreatment can attenuate the antibiotics tolerance of *P. aeruginosa*

Given that PYO exposure has been reported to induce the antibiotics tolerance of *P. aeruginosa*, especially on fluoroquinolones[37], we thus tested the effect of TET or TCS-pretreatment on the antibiotic tolerance of PAO1. The Δ*mexL* and Δ*phz* mutants were used as control strains due to their low PYO production. Unexpectedly, the Δ*mexL* mutant exhibited less tolerance to both Tobramycin (TOB) and Ciprofloxacin (CIP) (Fig. 6f), while the Δ*phz* is less tolerant to CIP, but not to TOB, which is consistent with the previous report[37]. Strikingly, the TCS-pretreatment at sub-inhibitory concentrations significantly increased the sensitivity of PAO1 to both CIP and TOB, reaching a level similar to that of Δ*mexL* (Fig. 6f). TET-pretreatment also reduced the tolerance of PAO1 to CIP, but not to TOB (Fig. 6f). These data suggest that TET and TCS can also be used to enhance sensitivity of PAO1 to antibiotics, such as CIP and TOB.

The combination of TET or TCS with clinical antibiotics enhances the survival rate of mouse in an intratracheal infection model

We next tested whether an administration of TET or TCS combined with CIP or TOB could efficiently cure *P. aeruginosa* infections. We first examined the combined efficacy of antibiotics against PAO1 using a chequerboard assay. No synergy or antagonism was observed between TET with CIP (FICi = 2.0) or TOB (FICi = 1.5), TCS with CIP (FICi = 0.53) or TOB (FICi = 1.25) (Figure S7), while TCS combined with CIP showed additive effects. This indicated that all these combinations can be used.

We then examined the antimicrobials combinations in a murine intratracheal infection model to treat *P. aeruginosa* infections (Fig. 7a). Different antibiotics treatments were performed in the PAO1-infected mice at 1 dpi. TET and TCS were used at a half amount of regular concentration (marked as $TET_{1/2}$ and $TCS_{1/2}$) for a purpose of reducing the virulence of *P. aeruginosa*. $TET_{1/2}$ and CIP combination showed the best survival rate among all antibiotics treatments (50% at 5 dpi, Fig. 7b), followed by the $TET_{1/2}$ and TOB combination (40% at 5 dpi, Fig. 7b), which was consistent with the result of antibiotic tolerance assay (Fig. 6f). The Δ*mexL* mutant-infected mice without antibiotics treatment had 20% survival rate at 5 dpi (Fig. 7b) even if the Δ*mexL*-infected mice had higher bacterial burdens in the lung than the PAO1-infected mice at 1 dpi (Fig. 7c). The PAO1-infected mice without antibiotics treatment were all dead at 3 dpi, while $TET_{1/2}$, $TCS_{1/2}$, TOB, or CIP treatment groups were all dead at 4 dpi. (Fig. 7b). The in vitro assay indicated that the TCS with CIP was the best combination (Fig. 6b), yet in this infection model, $TCS_{1/2}$ with CIP only gave 13% survival rate at 5 dpi (Fig. 7b). This was likely due to the limited solubility of TCS in water. As shown in Figure S4, TOB did not interfere with the DNA-binding of MexL, thus we also set up the treatment of $TOB_{1/2}$ and CIP combination, which showed 0% survival rate at 5 dpi (Fig. 7b) although the in vitro assay indicated no antagonism for this antibiotic combination (Fig. 6b). These results suggest that only the antibiotics interfering with MexL can increase the survival rate when they were used in combination with another clinical antibiotic against *P. aeruginosa* infection. The survival rates were well correlated with bacterial load, expression level of pro-inflammatory cytokines in the murine lungs, and histological examinations of the lung lobes (Figs. 7c–e and Figure S8). In addition, the results also further confirmed that the Δ*mexL* strain was less virulent than the wild type strain PAO1. Taken together, our data reveal that the MexL-targeted compounds can reduce the pathogenesis of *P. aeruginosa* and the animal survival rate is significantly enhanced by the treatments that combining an antimicrobial targeting MexL with the antibiotics that are often used to combat *P. aeruginosa* infection. The homolog of MexL was found in all *Pseudomonas* species with genomic sequences (Figure S9). Moreover, MexL was highly conserved among 65 *P. aeruginosa* strains isolated from either clinic or environment (Figure S9), suggesting that antibiotics combinations we have shown above could be a common strategy to combat *P. aeruginosa* infections.

Discussion

P. aeruginosa is one of the most common pathogens that cause nosocomial infections. It is in high priority to develop new antibiotics for this pathogen, especially for the carbapenem-resistant *P. aeruginosa*[38]. Discovery of new drug targets would be a great help for the development of new strategies or antibiotics to control *P. aeruginosa* infections. Phenazine PYO is an important virulence factor of *P. aeruginosa* that can enhance the survival of this pathogen during infections. This pigment is also an antimicrobial compound that can inhibit the growth of many microorganisms, which enables *P. aeruginosa*, the phenazine producer, to outcompete other microorganisms in a multiple microbial environment[39]. PYO can also promote biofilm formation and mediate antibiotic tolerance in *P. aeruginosa*[37,40]. Therefore, reducing PYO production could be a way to control *P. aeruginosa* infections. In this study, we report a novel drug target, MexL that can control PYO production of *P. aeruginosa* and find antimicrobials that can interfere with MexL to reduce the virulence of this pathogen.

Efflux pumps are the major strategies for bacteria to protect themselves from toxic compounds and meanwhile confer increased resistance to antibiotics. Some efflux pumps have been reported to be involved in transport of phenazines, secondary metabolites produced by *P. aeruginosa*[23]. Previous publications have showed that the production of phenazine PYO is mainly regulated by QS regulation system. Up to date, efflux pump regulator has not been shown to directly control PYO biosynthesis. In this report, we have provided a novel regulatory mechanism of *P. aeruginosa* to control phenazines' biosynthesis. We have shown that MexL, the transcriptional repressor of the multidrug efflux pump MexJK, can directly bind the promoter of several phenazine biosynthesis genes to activate the PYO production. Furthermore, PYO functions as a terminal signal that negatively autoregulates its own expression via MexL, especially under the condition with high concentration of PYO. This negative feedback regulatory mechanism may protect *P. aeruginosa* from the overproduction of phenazine and antibiotics that may interfere with MexL.

Furthermore, our results reveal that MexL is a potential drug target because MexL knockout strain is less virulent than the wild type strain. This is indicated by the ability of the Δ*mexL* mutant on the killing of other bacteria, human epithelial cells, or mice in an acute pneumonia animal model. More importantly, the Δ*mexL* strain induces less antibiotic tolerance than its parental strain. Crystal structure analysis reveals that MexL is a typical TetR family regulator containing a DNA binding domain and a ligand binding domain. PYO can directly

https://doi.org/10.1038/s41467-025-57294-8

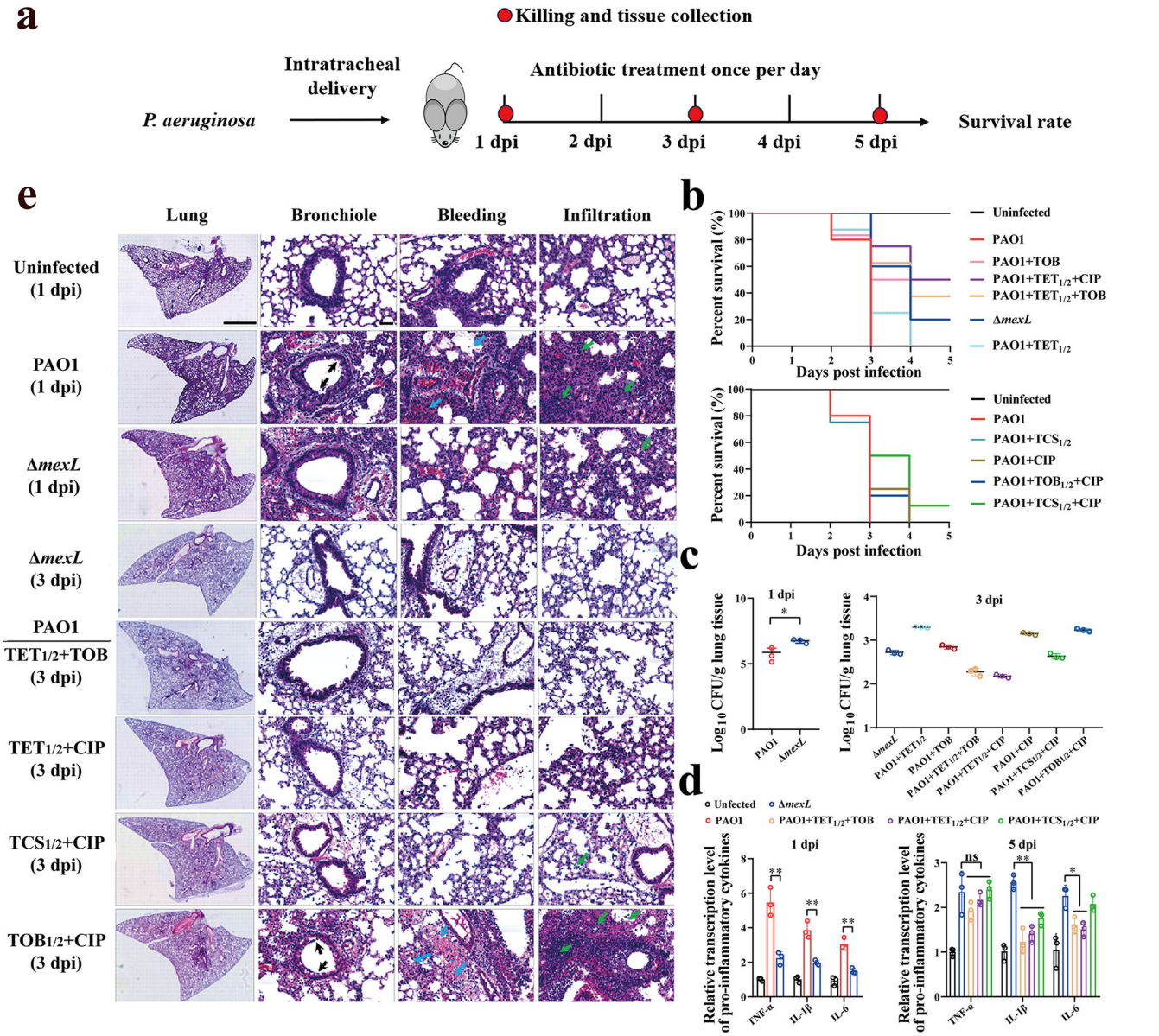

Fig. 7 | Mouse acute pneumonia model to determine the antibiotic combinations against *P. aeruginosa* infection. a Experimental design for *P. aeruginosa* infection and antibiotics treatment. **b** The survival rate of the intratracheal infected mice ($n = 8$/group). One day post-infection, the PAO1-infected mice were treated with $TET_{1/2}$, TOB, $TET_{1/2}$ + TOB, $TCS_{1/2}$, CIP, $TCS_{1/2}$ + TOB, $TET_{1/2}$ + CIP, $TOB_{1/2}$ + CIP for 3 days, respectively. The PAO1 and Δ*mexL* infected groups without antibiotic treatment serves as the control. The mice were monitored once daily for morbidity and mortality for 5 days. $TET_{1/2}$, $TCS_{1/2}$, and $TOB_{1/2}$ represent half of the normal dosage of corresponding antibiotics. **c** Bacterial burden was evaluated in lungs of the intratracheal infected mice at 1day post-infection (1 dpi) and 3 days post-infection (3 dpi). ($n = 3$ independent experiments). **d** Expression levels of pro-inflammatory cytokines in the murine lungs of the intratracheal infected mice at 1 dpi and 5 dpi respectively. ($n = 3$ independent experiments). **e** Histological examination of lung tissue sections from the intratracheal infected mice at 1 dpi and 3 dpi. The representative sections were shown. The images in left panel were the representative section of lung tissue from each treatment group. The other images were selected to show the detail of pathogenicity. The black arrows represent the loss of airway epithelial integrity. The blue arrows represent the lung parenchyma damage with bleeding. The green arrows represent inflammatory infiltration. Scale bar, 2 mm in the left panel; 50 μm in the other panels. *P* values were determined using two-tailed Student's *t* test. Significance was indicated by a *P* value. ns, non-significant, $^{**}P < 0.01$, $^{*}P < 0.05$. **c** $P = 0.015$ (PAO1 vs Δ*mexL*). **d** $P = 0.00345$ (TNF-α, 1 dpi), 0.003 (IL-1β, 1 dpi), 0.0021 (IL-6, 1 dpi), 0.00196 (Δ*mexL* vs PAO1 + $TET_{1/2}$ + TOB, IL-1β, 5 dpi), 0.00122 (Δ*mexL* vs PAO1 + $TET_{1/2}$ + CIP, IL-1β, 5 dpi), 0.0033 (Δ*mexL* vs PAO1 + $TCS_{1/2}$ + CIP, IL-1β, 5 dpi), 0.0184 (Δ*mexL* vs PAO1 + $TET_{1/2}$ + TOB, IL-6, 5 dpi) and 0.0107 (Δ*mexL* vs PAO1 + $TET_{1/2}$ + CIP, IL-6, 5 dpi).

interact with MexL likely at the ligand binding domain. PYO-MexL interaction might cause a change in 3D structure, leading to a loss of DNA binding function of MexL and a decrease of PYO production. This explains the molecular basis for PYO as a feedback signal. Meanwhile these results have guided us to find two antimicrobials, TET and TCS, which might also interact with the ligand binding domain of MexL at the similar position as PYO. Strikingly, these two drugs at sub-inhibitory concentrations can not only reduce the PYO production, but also attenuate the virulence and antibiotic tolerance of *P. aeruginosa*. These results further lead to a strategy for combating *P. aeruginosa* infection, which is by using drugs or antimicrobials that interfered with the function of MexL (such as TET or TCS) to reduce the virulence of *P. aeruginosa* and host inflammatory reposes, resulting in the improvement of *P. aeruginosa* clearance by clinical antibiotics. A very

recent report has promoted that the overexpression of efflux pumps in *P. aeruginosa* can decrease pathogenesis[41]. TET treatment can induce the overexpression of the efflux pump MexJK (10 times higher than no treatment control, Figure S4b), which could be another reason for why TET treatment has given the best result in decreasing *P. aeruginosa* pathogenesis.

Our data not only demonstrate a novel regulatory mechanism, but also provide a drug target, MexL in *P. aeruginosa*. We have also revealed a new role for old antimicrobials (TET and TCS), which can act as the virulence reducer for *P. aeruginosa*. Furthermore, our results also provide antibiotics combinations to treat *P. aeruginosa* related infections. Amino acids sequence alignment has revealed MexL homologs in several pathogens (Figure S10), including *Escherichia coli*, *Acinetobacter baumannii*, *Klebsiella pneumoniae*, and *Salmonella enterica*, etc. It would be worth investigating in the future whether these MexL homologs can be used as the targets for combating infections caused by corresponding pathogens.

Methods

Ethics statement

All animal studies were carried out under the Guide Protocol of Laboratory Animals (SIAT-IACUC-20211201-YYS-DXS22X-LL-A2056-01) and approved by the Ethics Committee of the Shenzhen Institute of Advanced Technology Chinese Academy of Sciences. Mice used in this study were female BALB/c mice aged 6–8 weeks or C57BL/6 mice aged 8 weeks old. Mice were housed in cages with ad libitum food and water. The room was maintained at a temperature of 21 °C, with 45-65% humidity on a 12-hour light-dark cycle.

Strains and growth conditions

The Supplementary Data 1 provided the information of the strains, plasmids, primers, chemicals and antibiotics used in this study. Unless otherwise indicated, *P. aeruginosa* and *E. coli* were grown in Luria-Bertani (LB) medium at 37 °C with shaking. When required, selective antibiotics were added into the medium. Antibiotics were used at the following final concentrations: for *E. coli* with pET28a, kanamycin at 50 μg/mL; for *E. coli* with pROBE-AT' and pUCP20, ampicillin at 100 μg/mL; for *E. coli* with pEX18Gm, gentamicin at 10 μg/mL; for *P. aeruginosa* with pROBE-AT' or pUCP20, carbenicillin at 300 μg/mL. For the effect of sub-inhibitory concentration of antibiotic on *P. aeruginosa*, tetracycline (TET) was used at a final concentration of 10 μg/mL (20 μM), 15 μg/mL (30 μM), or 20 μg/mL (40 μM), respectively; triclosan (TCS) was used at the final concentration of 32 μg/mL (110 μM), 64 μg/mL (220 μM), or 128 μg/mL (440 μM), respectively.

Construction of *P. aeruginosa* mutants and complementation strains

The in-frame deletion mutant strains in *P. aeruginosa* PAO1 were constructed by two-step allelic exchange as described previously with minor modifications[42]. Briefly, upstream and downstream DNA region of the targeted gene were amplified by PCR and fused with overlapping PCR. Then the PCR products were cloned into the vector pEX18Gm to generate the recombinant plasmid pEX18Gm-*mexL*. The *E. coli* S17-1 *λpir* contained the recombinant vectors served as delivery strain for the chromosome integration of PAO1. The deletion mutants were confirmed by PCR and DNA sequencing. For construction of the complementation strains, the *mexL* gene was amplified by PCR, and then cloned into the shuttle plasmid pUCP20, yielding the recombinant plasmid pMexL, which was sequenced and transformed into the *mexL* deletion mutants.

Antibiotic susceptibility analysis

The determination of minimum inhibitory concentrations (MIC) for triclosan (TCS) and tetracycline (TET) against PAO1, Δ*mexL* and Δ*mexJK* were performed as previously described with minor modifications[43]. Briefly, the strains were cultured in LB medium at 37 °C until the OD_{600} reached 0.6, then diluted 100-fold into fresh LB medium. 100 μL aliquots of which were transferred into the 96-well plate. A serial of two-fold dilutions of the antibiotics were added into columns with bacterial cultured in LB medium. Culture without any antibiotics was applied as the negative control. The plates were incubated on the micro-plate shaker at 37 °C for 16 h. The MIC values of each antibiotic were determined as to indicated drug concentration that inhibited at least 99% of bacteria growth.

Measurement of pyocyanin production

Pyocyanin was extracted from culture supernatant and measured according to the previously reported methods[44,45]. Briefly, *P. aeruginosa* strains were grown in LB medium for 16 h. 5 mL of culture supernatant was added into a 15 mL tube containing 3 mL of chloroform, and mixed with vortex for 10 min, The chloroform layer in the bottom was transferred to a new 5 mL tube, and 1 mL of 0.2 M HCl was then added into the chloroform and mix well by vortex. The upper pink layer of liquid was collected and subjected to measurement at 520 nm.

Biofilm assay

Microtiter biofilm assay was performed as previously described with modifications[46]. Briefly, overnight culture was diluted with 1:100 in Jensen's medium (unless other specific medium is required), and grown in a polyvinylchloride plate (Costar) at 25 °C (unless other specific temperature is required) for 24 h. Surface-attached bacteria were stained with 0.1% crystal violet at room temperature for 15 min, and washed twice by dipping into standing water bath. The adherent stain was solubilized in 40% acetic acid and quantified by measuring its optical density at 560 nm.

RNA isolation and quantitative RT-qPCR analysis

For RNA isolation, the wild type PAO1, *mexL* deletion and complementary strains were cultured in LB medium at 37 °C until the OD_{600} reached 2.5-3.0 (early stationary phase). 0.5 mL of bacteria cultures of each strain were harvested, and total RNA was exacted using the total bacteria RNA Extract Kit (Tiangen, Beijing, China). cDNA was synthesized using the high-capacity reverse transcription kit (Tiangen, Beijing, China). Quantitative real-time PCR was performed using the Light Cycler 480 (Roche). The 30S ribosomal protein gene *rpsL* was used as a control gene for normalization. The effect of PYO, TET, TCS and TOB on the *mexJ* transcription level was determined as previously reported with minor adjustments[15,37,39]. Briefly, PAO1 or Δ*mexL* was allowed to grow to exponential phase (OD_{600} = 0.5) in LB medium at 37 °C, then corresponding concentration of PYO (250 μM, 500 μM), TET (300 μM, 5 × MIC), TCS (3000 μM, > 5 × MIC) and TOB (10 μM, 5 × MIC) were added into the culture and treated for 3 h respectively. PAO1 or Δ*mexL* cultured without treatment was used as the control. The bacteria were collected, and total RNA was extracted for RT-qPCR.

LC-MS/MS analysis of phenazines

The extraction of PCA and PYO and their quantification by LC-MS/MS were performed as previously described[23]. Briefly, the cultures were grown in LB medium to the late stationary phase (OD_{600} = 4.5), centrifuged at 11,000 *g* for 5 min, and the supernatant was filtered through 0.22 μm PES membrane. The supernatant was diluted 100 times in acetonitrile and analyzed by LC-MS/MS. A 10 μL of aliquot was loaded on mass spectrometer (QTRAP 6500 System, AB SCIEX). The standard PCA (Macklin, China) and PYO (Cayman, USA) were diluted into a linear dynamic range of concentrations (0.1 μg/mL,1 μg/mL, 5 μg/mL, 10 μg/mL, 50 μg/mL and 100 μg/mL), and the standard curve was obtained between peak area and the concentration of PCA or PYO standard. The contents of PCA or PYO were calculated through the standard curve.

Protein expression and purification

The *mexL* was amplified from PAO1 genomic DNA by PCR, cloned into the plasmid pET28a between the BamHI and HindIII sites, and confirmed by DNA sequencing. The pET28a-*mexL* was transformed into *E. coli* BL21 (DE3) for protein expression. The overnight cultures were transferred into 500 mL fresh LB medium supplemented with 50 μg/mL kanamycin and incubated with shaking (200 rpm) at 37 °C until OD_{600} reached ~0.6. The strains were induced with 0.1 mM isopropyl-β-D-thiogalactoside (IPTG) for 16 h at 25 °C. Bacterial cells were harvested and resuspended in 50 mL of lysis buffer (10 mM PBS, 100 mM NaCl) and disrupted by sonication for 30 min. The cell debris were removed by centrifugation at 9500 × *g* for 30 min at 4 °C, and the supernatant was filtered through Ni-NTA column (Bio-Rad). The column was pre-washed with 10 mL of lysis buffer, then with the washing buffer (10 mM PBS, 100 mM NaCl, and 60 mM imidazole, pH 8.0) prior to the sample loading. The target protein was eluted with elution buffer (10 mM PBS, 100 mM NaCl, and 250 mM imidazole, pH 8.0). The purified proteins were examined by SDS-PAGE, and desalted with 10 mM PBS to remove the imidazole at 4 °C. The protein samples were supplemented with 5% glycerol (final concentration), and stored at -80 °C for further use. The concentrations of protein were measured by BCA method.

Protein crystallization, data collection and structure determination

Because the full-length MexL protein failed to form good crystals, the N-terminal first 14 residues of MexL were truncated, and the expression product was named $MexL_{15\text{-}212}$ and used for crystallization. The purification of $MexL_{15–212}$ was carried out as described above (see Protein expression and purification) with minor adjustments. The eluted protein was dialyzed against dialysis buffer (20 mM Tris-HCl pH 8.0, 150 mM NaCl) and then incubated with thrombin for 2 h at 4 °C to remove the His tag. The digestion mixture was reloaded into the Ni-NTA affinity column. The tag-free protein was eluted from the resin in dialysis buffer supplemented with 20 mM imidazole. The protein was further purified by passing through a HiLoad 16/600 Superdex 200 prep-grade column (GE healthcare) in GF buffer (20 mM Tris-HCl pH 8.0, 100 mM NaCl). Peak fractions containing $MexL_{15\text{-}212}$ were concentrated to ~15 mg/mL using an Amicon Ultra−10 K (Millipore), flash-frozen in the liquid nitrogen, and kept at −80 °C for future uses. Initial crystallization screening was performed using the commercial crystallization screening kits using sitting drop vapor diffusion method at 18 °C. Each drop was prepared by mixing 1 μL of protein solution with 1 μL of reservoir solution and sealed in a well containing 70 μL of reservoir solution. Romboid crystals were obtained in condition containing 0.14 M K_2HPO_4, 1.26 M NaH_2PO_4 within 7 days and were further optimized by seeding. Crystals were transferred into a cryoprotectant solution consisting of 25% (v/v) glycerol in the reservoir solution and flash frozen in liquid nitrogen for diffraction data collection. The crystallographic data sets were collected on the beamlines 19U1 at the Shanghai Synchrotron Radiation Facility (SSRF)[47]. The diffraction images were processed using XDS[48]. The structure of $MexL_{15\text{-}212}$ was solved by molecular replacement using a structure predicted by AlphaFold2[35] as the model. The initial model of $MexL_{15\text{-}212}$ was built using AutoBuild[49] and manually adjusted using Coot[50]. The iterative refinement and structure validation were done using Phenix[51]. The data collection and refinement statistics of $MexL_{15\text{-}212}$ were shown in Table 1. A portion of the electron density map of the solved $MexL_{15\text{-}212}$ crystal structure was shown in Figure S11.

Site-directed mutagenesis

The recombinant plasmid pET28a-*mexL* and pMexL were used as the PCR template, and PCR reaction was performed with supplement of specific primers for the desired mutation. PCR products were digested with *Dpn*I (NEB) to remove the parental supercoiled dsDNA, and then transformed into *E. coli* DH5α to generate recombinant plasmids with mutation. Identification of the mutations was validated by DNA sequencing.

Electrophoretic mobility shift assays (EMSA)

The promoter DNA fragments of target genes (~500 bp upstream regions from the start codon) were amplified by PCR. The purified MexL or MexL mutant proteins were incubated with promoter DNA (20 nM) in a binding reaction buffer (10 mM Tris-HCl, PH 7.5, 50 mM KCl, 1 mM DTT, 100 ng/μL Poly-DI DC) for 30 min at room temperature with the final volume of 20 μL, respectively. The samples were analyzed by 6% native polyacrylamide gels electrophoresis in 0.5 × TBE buffer at 100 V for 1 h. Then, the gels were stained with nucleic acid dye for 5 min, and visualized using the gel imaging system (Bio Rad, USA). Promoter of *mexJ* and *mexL* was used as the positive control, and 30S ribosomal protein gene *rpsL* promoter was used as the negative control. To study the effect of PCA, PYO, TCS, TET and TOB on the binding capacity of MexL and promoter, corresponding concentrations of PYO, PCA, TCS, TET and TOB were added to the EMSA reaction system, respectively.

The shortest MexL-binding regions (about 50 bp, named BS-*mexJ*, BS-*phz1*, BS-*phz2*, and BS-*phzM*, respectively) used in the EMSA system, were obtained by 5′-FAM (carboxyfluorescein) labeled-forward primer and non-labeled reverse primer annealing. 20 nM FAM-labeled DNA and 40 μM MexL protein were added into the EMSA reaction buffer (10 mM Tris-HCl, PH 7.5, 50 mM KCl, 1 mM DTT, 100 ng/μL Poly-DI DC) for 30 min at room temperature. Then sample were subjected to 6% native polyacrylamide gels in 0.5 × TBE buffer at 100 V for 1 h. The gels were visualized by Typhoon 9500 FLA scanner (GE Healthcare).

Microscale thermophoresis measurement

MST experiments were conducted based on the previously report method with minor modifications[52]. Briefly, the 5′-FAM (carboxyfluorescein) labeled DNA fragments containing the promoter regions of *mexJ*, *phz1*, *phz2* and *phzM* were amplified from PAO1 genomic DNA, respectively. A serial 2-fold dilution of MexL (460 μM to 0.014 μM) were used for the assay. The purified DNA fragments at 10 μL were mixed with 10 μL of different concentration of MexL, respectively, and the 4 μL of such mixtures were loaded on standard treated silicon capillaries (NanoTemper, MO-K002), the measurements were carried out using Monolith NT.115 instrument (NanoTemper Technologies GmbH, Germany). The dissociation constants (K_D) were calculated using the Nanotemper Analysis software.

Nano differential scanning fluorimetry (nanoDSF)

The thermal stability of MexL in the presence of PCA and PYO was determined using nano-differential scanning fluorimetry (nanoDSF), which bases on the intrinsic fluorescence of aromatic amino acids tryptophan and tyrosine in protein[53]. Samples were measured by Prometheus NT.48 (NanoTemper Technologies GmbH, Germany). Briefly, 10 μM purified MexL was mixed with PCA or PYO at final concentrations of 50, 250, and 500 μM, respectively. The sample MexL mixed with water was used as control. After being incubated at room temperature for 10 min. Then each sample was filled into Prometheus NT.48 standard capillary, and placed into the sample holder. The temperature range was set from 25 °C to 95 °C at a ramp rate of 1 °C/min. The emission intensities at 330 nm and 350 nm were recorded, which reflect the shift of intrinsic fluorescence of proteins upon temperature-induced unfolding. The thermal unfolding curves were obtained, and melting temperature (T_m) values of the MexL were generated from the first derivative of the ratio at Em_{350}/Em_{330}.

Biolayer interferometry assays

The binding affinity between MexL and PYO were determined by Biolayer interferometry (BLI) experiments, and performed in an Octet Red 96 instrument (ForteBio). The 10 μM of MexL was labeled by

NHS-PEG12-Biotin (Sigma) in the PBST reaction buffer (1 × PBS, 0.02% tween 20) at 4 °C for 1 h. After reaction, free biotin was removed by using a 10 K spin desalt column. Biotinylated MexL was immobilized on streptavidin biosensors and incubated with PYO in PBST buffer. The PYO was two-fold-serial diluted for 6 dilutions (500, 250, 125, 62.5, 31.25 and 15.63 μM). Data were analyzed with Octet Data Analysis Software (ForteBio). The response of the sensor from three independent measurements at each PYO concentration was plotted and binding affinity K_D was determined.

A549 lung epithelial cells infection model

The lung epithelial cell A549 was purchased from the Beijing Solarbio Technology Co., LTD (Cat: SCC-110411, China), and cultured in DMEM medium (Gibco; C11965500BT) containing 10% fetal bovine serum (FBS, VivaCell; C04001) in cell culture supplied with 5% CO_2 at 37 °C as the instruction provided by the company. A549 cells were plated 12 h before infection in 24 -well plates at 2.5×10^5 cells per well. *P. aeruginosa* were grown in LB medium at 37 °C until the OD_{600} reaches 0.6. A549 cells were washed once with DMEM-FBS and resuspended in DMEM-FBS medium. *P. aeruginosa* infection was performed at a multiplicity of infection (MOI) of 50. After 5 h post-infection, cells were harvested using 0.025% Trypsin/EDTA, washed once with PBS, and resuspended in PBS for subsequent manipulation. Cells were stained according to protocols of the FITC Annexin V Apoptosis Detection Kit with 7-AAD (Biolegend). The samples were analyzed by flow cytometry (BD influx system, BD Bioscience).

The A549 cell viability detection was performed according to the cell counting kit-8 (CCK8, Dojindo, Japan), which detects cellular dehydrogenase activity in living cells. The PAO1 and Δ*mexL* were grown in LB medium containing tetracycline (TET, 30 μM) or triclosan (TCS, 220 μM) for 16 h at 37 °C. PAO1, Δ*mexL* and Δ*phz* without any antibiotic were grown at same conditions as controls. All the strains were washed three times with PBS and resuspended in PBS to an OD_{600} of 1.0. The bacteria and A549 cells were incubated at 37 °C for 24 h, followed by the CCK-8 assay to determine the living cells viability. The A549 cells without *P. aeruginosa* infected served as the control. Cell viability was calculated according to the following formula: Cell viability (%) = [A test / A control] ×100%.

Molecular docking

The program AutoDock 4.2 was used to predict the binding modes of three substrates, PYO, TCS and TET, in the MexL protein. The $MexL_{15-212}$ dimer structure was used for docking. The protein was set as a rigid structure, whereas the conformation of each substrate molecule was optimized via all modeling and docking procedures.

Animal infection models

For examination of *P. aeruginosa* pathogenicity on mice, infection of mice was performed as described previously[54]. BALB/c Mice (SPF Biotechnology CO., LTD., Beijing, China) aged 6–8 weeks were selected for 3–5 days of adaptive feeding. After random grouping, the weight of the mice was measured. Prior to infection, the mice were anesthetized by tribromoethanol (1.25%) (Beijing Laboratory Animal Research Center, Beijing, China) via intraperitoneal injection at a dose of 0.2 mL/10 g body weight. The overnight culture of *P. aeruginosa* was diluted with PBS to 10^8 colony-forming units (CFU)/mL. The 20 μL of bacterial suspension was intranasally inoculated into each mouse (10 μL for each nostrils). Survival and weight of the mice was monitored and recorded every 24 h for 6 days. One day 1 post-infection, three mice were sacrificed and their lungs were dissected for the enumeration of bacterial CFU and the H&E staining (hematoxylin and eosin). After six days' post-infection, all mice were sacrificed. Lungs were dissected for the enumeration of bacterial CFU and the H&E staining.

The murine intratracheal infection model was performed as described previously with modifications[55]. C57BL/6 Mice aged 8 weeks were selected for adaptive feeding for 3-5 days. Before infection, mice were anesthetized using ketamine (80 mg/kg body weight) and xylazine (10 mg/kg body weight). The mice were infected intratracheally with the *P. aeruginosa* suspension with 2×10^7 CFU in 60 μL of PBS. One day post-infection, PAO1-infected mice were treated by 0.9% saline (control group, 200 μL per mouse), tetracycline (TET, 10 mg/kg), tobramycin (TOB, 30 mg/kg), tetracycline (TET, 10 mg/kg) and tobramycin (TOB, 30 mg/kg), tetracycline (TET, 10 mg/kg) and ciprofloxacin (CIP, 10 mg/kg), triclosan (TCS, 50 mg/kg), ciprofloxacin (CIP, 10 mg/kg,), triclosan (TCS, 50 mg/kg) and ciprofloxacin (CIP, 10 mg/kg), tobramycin (TOB, 15 mg/kg) and ciprofloxacin (CIP, 10 mg/kg) respectively once per day for 3 days through intraperitoneal injection. Survival of mice was monitored and recorded every 24 h for 5 days. Three mice from each group (uninfected, PAO1-infected, and Δ*mexL* mutant-infected) at 1 dpi and all survival mice at 3 or 5 dpi were sacrificed and their lungs were dissected for the enumeration of bacterial CFU, the H&E staining (hematoxylin and eosin), and total RNA extraction.

Chequerboard broth microdilution assays

Chequerboard analyzes were conducted using the 96-well-plates method as described with slight modifications[56]. Briefly, the overnight bacterial culture of *P. aeruginosa* PAO1 was diluted to an OD_{600} of 0.1, then 1% inoculated into fresh LB containing 2-fold dilutions of each antibiotic in a 5 × 5 dose-point matrix. The plates were incubated at 37 °C overnight, and the absorbance of OD_{600} was measured. At least three biological replicates were completed for each combination. Heat maps were generated according to OD_{600}, and the FIC indices (FICi) for the two compounds (A and B) were calculated. FICi = [MIC of antibiotic A in combination with antibiotic B/ MIC of antibiotic A alone] + [MIC of antibiotic B in combination with antibiotic A/ MIC of antibiotic B alone]. The interactions were interpreted based on the calculation of FICi, in which: FICi ≤ 0.5, synergistic; 0.5≤ FICi ≤ 1, additive; 1≤ FICi ≤ 2, neutral; and FICi > 2, antagonistic, respectively.

Antibiotic tolerance assay

The antibiotic tolerance assay of PAO1 against CIP and TOB was conducted following the protocol described with minor modifications[37], Δ*mexL* and Δ*phz* were used as negative controls. Briefly, each overnight bacterial culture was grown in M9 minimal medium supplied with 20 mM glucose. Next, the bacterial cells were pelleted, washed, and resuspended in M9 medium containing 10 mM glucose to reach OD_{600} of 0.05. Five corresponding treatments were prepared: PAO1, PAO1 cultured with 30 μM TET, PAO1 cultured with 220 μM TCS, Δ*mexL* and Δ*phz*, then incubated at 37 °C for 20 h. Each individual culture was then split into a negative control (no antibiotic) or antibiotic treatment (1 μg/mL CIP or 4 μg/mL TOB), and incubated at 37 °C for 4 h. Then, surviving cells were serially diluted and plated on LB agar plate to determine the viable CFUs. The bacterial survival rate (%) = [number of colonies with antibiotic treatment / number of colonies without antibiotic treatment] × 100%.

S. aureus plate killing assay

The bactericidal activity of *P. aeruginosa* against *S. aureus* was performed as described previously with slight modification[57]. The PAO1, *mexL* mutants and complementary strains were cultured overnight at 37 °C in LB and 10 mL of supernatants were collected by centrifugation. The secondary metabolites were extracted from supernatants with 5 mL of chloroform, died, and resuspended in 500 μL of methanol. An overnight culture of *S. aureus* strain NCTC 8325 was grown in LB, then diluted to fresh liquid medium to OD_{600} = 0.1, evenly spread on the surface of LB agar. 20 μL of *P. aeruginosa* extract was spotted on 5.5 mm-diameter Whatman filter paper placed on the *S. aureus* plate, and incubated for 24 h at 37 °C, and the diameter of the inhibition zone was measured.

Swarming motility

The strains PAO1, PAO1 cultured with 30 μM TET or 220 μM TCS, Δ*mexL*, Δ*mexL* cultured with 30 μM TET or 220 μM TCS were grown in LB medium at 37 °C for 16 h. Swarming motility was performed in Nutrient Broth with 0.5% glucose and 0.5% Difco Bacto agar as previously reported[58]. The plates were placed in an incubator at 37 °C overnight until swarming zones were formed. Then, the plates were imaged and the swarming zone (cm^2) was analyzed by Image J software.

Western blot

Western blot was performed according to previous reports with slight modification[59]. Briefly, overnight culture of PAO1/pBAD-MexL was diluted 1:100 in LB medium, then divided into three parts, namely no antibiotic treatment, 30 μM TET treatment, and 220 μM TCS treatment. The bacteria were allowed to grow for 2 h, then arabinose (1% final concentration) was added and was continued to grow for 16 h. The bacteria were collected, washed with PBS, resuspended in 1 mL of PBS, and disrupted by sonication. Samples were centrifuged at 9500 × *g* for 10 min, and the supernatant was transferred into a new sample tube, mixed with 5 × SDS-PAGE sample buffer, boiled for 10 min and centrifuged at 9500 × *g* for 10 min. Proteins were separated by a 12% SDS-PAGE gel and transferred to a PVDF membrane. RNA polymerase (RNAp) was detected by anti-RNAp antibody (Abcam, Inc., ab191598) and served as an internal control. The MexL was detected by anti-MexL antibody (made by Abmart Inc., Shangai, China). The PVDF membrane were photographed with a gel imaging system and for further analysis.

Fluorescence-based promoter activity assay

The promoter-*gfp* transcriptional fusions reporter plasmid pROBE-AT' was used to detect the activity of target genes' promoter[60]. The -35 and -10 box sites in the promoter region of *phz1* and *phzM* were identified by the previous studies[61,62]. The -10 and -30 regions of *phzA2* promoter were predicted by online software BPROM (http://www.softberry.com). The promoter region of target gene was amplified by PCR, and cloned into pROBE-AT'. Recombinant plasmids were transformed into PAO1 and its-derived mutant strains, respectively. For promoter activity assay, overnight cultures of the reporter strains were diluted 100-fold into fresh LB medium containing 300 μg/mL carbenicillin at optical density at 600 nm of 0.1 and cultured at 37 °C with shaking. The fluorescence intensity (Excitation and Emission wavelength at 488 nm and 520 nm, respectively) and bacterial growth (OD_{600}) were captured with Synergy H4 hybrid reader (BioTek, USA).

Protein alignment and phylogenetic tree analysis

The MexL homology amino acid sequences were downloaded from the National Center for Biotechnology Information (NCBI, http://www.ncbi.nlm.nih.gov/). Multiple sequence alignment was performed using T-Coffee (https://tcoffee.crg.eu/apps/tcoffee/) combined with ESPript 3.0 software (https://espript.ibcp.fr/ESPript/ESPript/).

Statistical analysis and Reproducibility

All the data were analyzed by using GraphPad Prism 8. *P* values were determined using two-tailed Student's t test. Significance was indicated by a *P* value. ns, non-significant, $^{***}P < 0.001$, $^{**}P < 0.01$, $^{*}P < 0.05$. Error bars shown in the pictures represent ± SD (standard deviation) from at least three biological replicates. Representative images in figures were selected from at least three independent experiments.

Reporting summary

Further information on research design is available in the Nature Portfolio Reporting Summary linked to this article.

Data availability

The data that support the findings of this study are provided within the manuscript and its associated Supplementary Information/Source Data file. The atomic coordinate and structure factors of $MexL_{15\text{-}212}$ generated in this study have been deposited in the Worldwide Protein Data Bank (wwPDB) under the accession code 8WRF. The strains, plasmids used in this study are available upon request. Source data are provided with this paper.

References

1. Murray, C. J. L. et al. Global burden of bacterial antimicrobial resistance in 2019: a systematic analysis. *Lancet* **399**, 629–655 (2022).
2. Clatworthy, A. E., Pierson, E. & Hung, D. T. Targeting virulence: a new paradigm for antimicrobial therapy. *Nat. Chem. Biol.* **3**, 541–548 (2007).
3. Sadikot, R. T., Blackwell, T. S., Christman, J. W. & Prince, A. S. Pathogen-host interactions in *Pseudomonas aeruginosa pneumonia*. *Am. J. Respir. Crit. Care. Med.* **171**, 1209–1223 (2005).
4. Eichenberger, E. M. & Thaden, J. T. Epidemiology and mechanisms of resistance of extensively drug resistant gram-negative bacteria. *Antibiotics (Basel)* **8**, 37 (2019).
5. Ciofu, O., Moser, C., Jensen, P. & Høiby, N. Tolerance and resistance of microbial biofilms. *Nat. Rev. Microbiol.* **20**, 621–635 (2022).
6. WHO. WHO bacterial priority pathogens list, 2024: Bacterial pathogens of public health importance to guide research, development and strategies to prevent and control antimicrobial resistance. (World Health Organization, 2024).
7. Dietrich, L. E. P., Teal, T. K., Price-Whelan, A. & Newman, D. K. Redox-active antibiotics control gene expression and community behavior in divergent bacteria. *Science* **321**, 1203–1206 (2008).
8. Perry, E. K., Meirelles, L. A. & Newman, D. K. From the soil to the clinic: the impact of microbial secondary metabolites on antibiotic tolerance and resistance. *Nat. Rev. Microbiol.* **20**, 129–142 (2022).
9. Lau, G. W., Hassett, D. J., Ran, H. & Kong, F. The role of pyocyanin in *Pseudomonas aeruginosa* infection. *Trends Mol. Med.* **10**, 599–606 (2004).
10. Noto, M. J., Burns, W. J., Beavers, W. N. & Skaar, E. P. Mechanisms of pyocyanin toxicity and genetic determinants of resistance in *Staphylococcus aureus*. *J. Bacteriol.* **199**, e00221–17 (2017).
11. Ammann, C. G., Nagl, M., Nogler, M. & Coraça-Huber, D. C. *Pseudomonas aeruginosa* outcompetes other bacteria in the manifestation and maintenance of a biofilm in polyvinylchloride tubing as used in dental devices. *Arch. Microbiol.* **198**, 389–391 (2016).
12. Hassan, H. M. & Fridovich, I. Mechanism of the antibiotic action pyocyanine. *J. Bacteriol.* **141**, 156–163 (1980).
13. Baron, S. S. & Rowe, J. J. Antibiotic action of pyocyanin. *Antimicrob. Agents Chemother.* **20**, 814–820 (1981).
14. Price-Whelan, A., Dietrich, L. E. P. & Newman, D. K. Rethinking 'secondary' metabolism: physiological roles for phenazine antibiotics. *Nat. Chem. Biol.* **2**, 71–78 (2006).
15. Dietrich, L. E., Price-Whelan, A., Petersen, A., Whiteley, M. & Newman, D. K. The phenazine pyocyanin is a terminal signalling factor in the quorum sensing network of *Pseudomonas aeruginosa*. *Mol. Microbiol.* **61**, 1308–1321 (2006).
16. Ramos, I., Dietrich, L. E. & Price-Whelan, A. DK N. Phenazines affect biofilm formation by *Pseudomonas aeruginosa* in similar ways at various scales. *Res. Microbiol.* **161**, 187–191 (2010).
17. Balaban, N., Zhu, K., Chen, S., Sysoeva, T. A. & You, L. Universal antibiotic tolerance arising from antibiotic-triggered accumulation of pyocyanin in *Pseudomonas aeruginosa*. *PLoS Biol.* **17**, e3000573 (2019).
18. Costa, K. C., Glasser, N. R., Conway, S. J. & Newman, D. K. Pyocyanin degradation by a tautomerizing demethylase inhibits *Pseudomonas aeruginosa* biofilms. *Science* **355**, 170–173 (2017).

19. Mavrodi, D. V. et al. Functional analysis of genes for biosynthesis of pyocyanin and phenazine-1-carboxamide from *Pseudomonas aeruginosa* PAO1. *J. Bacteriol.* **183**, 6454–6465 (2001).
20. Lorusso, A. B., Carrara, J. A., Barroso, C. D. N., Tuon, F. F. & Faoro, H. Role of efflux pumps on antimicrobial resistance in *Pseudomonas aeruginosa*. *Int. J. Mol. Sci.* **23**, 15779 (2022).
21. Adamiak, J. W. et al. Loss of RND-type multidrug efflux pumps triggers iron starvation and lipid A modifications in *Pseudomonas aeruginosa*. *Antimicrob. Agents Chemother.* **65**, e0059221 (2021).
22. Dreier, J. & Ruggerone, P. Interaction of antibacterial compounds with RND efflux pumps in *Pseudomonas aeruginosa*. *Front. Microbiol.* **6**, 660 (2015).
23. Sakhtah, H. et al. The *Pseudomonas aeruginosa* efflux pump MexGHI-OpmD transports a natural phenazine that controls gene expression and biofilm development. *Proc. Natl Acad. Sci. USA* **113**, E3538–E3547 (2016).
24. Zgurskaya, H. I., Weeks, J. W., Ntreh, A. T., Nickels, L. M. & Wolloscheck, D. Mechanism of coupling drug transport reactions located in two different membranes. *Front. Microbiol.* **6**, 100 (2015).
25. Chuanchuen, R., Narasaki, C. T. & Schweizer, H. P. The MexJK efflux pump of *Pseudomonas aeruginosa* requires OprM for antibiotic efflux but not for efflux of triclosan. *J. Bacteriol.* **184**, 5036–5044 (2002).
26. Chuanchuen, R., Murata, T., Gotoh, N. & Schweizer, H. P. Substrate-dependent utilization of OprM or OpmH by the *Pseudomonas aeruginosa* MexJK efflux pump. *Antimicrob. Agents Chemother.* **49**, 2133–2136 (2005).
27. Amieva, R., Gil-Gil, T., Martínez, J. L. & Alcalde-Rico, M. The MexJK multidrug efflux pump is not involved in acquired or intrinsic antibiotic resistance in *Pseudomonas aeruginosa*, but Modulates the Bacterial Quorum Sensing Response. *Int. J. Mol. Sci.* **23**, 7492 (2022).
28. Harrington, N. E., Littler, J. L. & Harrison, F. Transcriptome analysis of *Pseudomonas aeruginosa* Biofilm Infection in an ex vivo pig model of the cystic fibrosis lung. *Appl. Environ. Microbiol.* **88**, e01789–01721 (2022).
29. Chuanchuen, R., Gaynor, J. B., Karkhoff-Schweizer, R. & Schweizer, H. P. Molecular characterization of MexL, the transcriptional repressor of the *mexJK* multidrug efflux operon in *Pseudomonas aeruginosa*. *Antimicrob. Agents Chemother.* **49**, 1844–1851 (2005).
30. Holm, L., Laiho, A., Törönen, P. & Salgado, M. DALI shines a light on remote homologs: one hundred discoveries. *Protein Sci.* **32**, e4519 (2023).
31. Werner, N. et al. The induction mechanism of the flavonoid-responsive regulator FrrA. *FEBS J.* **289**, 507–518 (2022).
32. Yeo, H. K., Park, Y. W. & Lee, J. Y. Structural basis of operator sites recognition and effector binding in the TetR family transcription regulator FadR. *Nucleic Acids Res.* **45**, 4244–4254 (2017).
33. Brooks, B. E., Piro, K. M. & Brennan, R. G. Multidrug-binding transcription factor QacR binds the bivalent aromatic diamidines DB75 and DB359 in multiple positions. *J. Am. Chem. Soc.* **129**, 8389–8395 (2007).
34. Schumacher, M. A. et al. Structural basis for cooperative DNA binding by two dimers of the multidrug-binding protein QacR. *EMBO J.* **21**, 1210–1218 (2002).
35. Jumper, J. et al. Highly accurate protein structure prediction with AlphaFold. *Nature* **596**, 583–589 (2021).
36. Su, C. C. et al. Cryo-electron microscopy structure of an *Acinetobacter baumannii* Multidrug Efflux Pump. *mBio* **10**, e01295–19 (2019).
37. Meirelles, L. A., Perry, E. K., Bergkessel, M. & Newman, D. K. Bacterial defenses against a natural antibiotic promote collateral resilience to clinical antibiotics. *PLoS Biol.* **19**, e3001093 (2021).
38. Hu, Y. et al. Emergence and expansion of a carbapenem-resistant *pseudomonas aeruginosa* clone are associated with plasmid-borne *bla* $_{KPC-2}$ and Virulence-Related Genes. *mSystems* **6**, e00154-21 (2021).
39. Fu, T. et al. Evolution of resistance to phenazine antibiotics in *Staphylococcus aureus* and its role during coinfection with *Pseudomonas aeruginosa*. *Acs. Infect. Dis.* **7**, 636–649 (2021).
40. Zhu, K., Chen, S., Sysoeva, T. A. & You, L. Universal antibiotic tolerance arising from antibiotic-triggered accumulation of pyocyanin in *Pseudomonas aeruginosa*. *PLoS Biol.* **17**, e3000573 (2019).
41. Chain, C. et al. A folate inhibitor exploits metabolic differences in *Pseudomonas aeruginosa* for narrow-spectrum targeting. *Nat. Microbiol.* **9**, 1207–1219 (2024).
42. Wei, Q. et al. Diguanylate cyclases and phosphodiesterases required for basal-level c-di-GMP in *pseudomonas aeruginosa* as revealed by systematic phylogenetic and transcriptomic analyses. *Appl. Environ. Microbiol.* **85**, e01194–19 (2019).
43. Andrews, J. M. Determination of minimum inhibitory concentrations. *J. Antimicro. Chemoth.* **48**, 5–16 (2001).
44. Essar, D. W., Eberly, L., Hadero, A. & Crawford, I. P. Identification and characterization of genes for a second anthranilate synthase in *Pseudomonas aeruginosa*: interchangeability of the two anthranilate synthases and evolutionary implications. *J. Bacteriol.* **172**, 884–900 (1990).
45. Liang, H., Li, L., Dong, Z., Surette, M. G. & Duan, K. The YebC family protein PA0964 negatively regulates the *Pseudomonas aeruginosa* quinolone signal system and pyocyanin production. *J. Bacteriol.* **190**, 6217–6227 (2008).
46. O'Toole, G. A. & Kolter, R. Initiation of biofilm formation in *Pseudomonas fluorescens* WCS365 proceeds via multiple, convergent signalling pathways: a genetic analysis. *Mol. Microbiol.* **28**, 449–461 (1998).
47. Zhang, W.-Z. et al. The protein complex crystallography beamline (BL19U1) at the Shanghai synchrotron radiation facility. *Nucl. Sci. Tech.* **30**, 170 (2019).
48. Kabsch, W. XDS. *Acta Crystallogr. D. Biol. Crystallogr.* **66**, 125–132 (2010).
49. Terwilliger, T. C. et al. Iterative model building, structure refinement and density modification with the PHENIX AutoBuild wizard. *Acta Crystallogr. D. Biol. Crystallogr.* **64**, 61–69 (2008).
50. Emsley, P., Lohkamp, B., Scott, W. G. & Cowtan, K. Features and development of Coot. *Acta Crystallogr. D. Biol. Crystallogr.* **66**, 486–501 (2010).
51. Adams, P. D. et al. PHENIX: a comprehensive Python-based system for macromolecular structure solution. *Acta Crystallogr. D. Biol. Crystallogr.* **66**, 213–221 (2010).
52. Zhang H., et al. The *Pseudomonas stutzeri*-specific regulatory non-coding RNA NfiS Targets *katB* mRNA encoding a catalase essential for optimal oxidative resistance and nitrogenase activity. *J. Bacteriol.* **201**, e00334-19 (2019).
53. Real-Hohn, A., Groznica, M., Loffler, N., Blaas, D. & Kowalski, H. nanoDSF: in vitro label-free method to monitor picornavirus uncoating and test compounds affecting particle stability. *Front. Microbiol.* **11**, 1442 (2020).
54. Song, Y. et al. Emergence of hypervirulent *Pseudomonas aeruginosa* pathotypically armed with co-expressed T3SS effectors ExoS and ExoU. *hLife* **1**, 44–56 (2023).
55. Li, L. et al. *Neisseria species* as pathobionts in bronchiectasis. *Cell Host Microbe* **30**, 1311–1327.e1318 (2022).
56. Carfrae, L. A. et al. Inhibiting fatty acid synthesis overcomes colistin resistance. *Nat. Microbiol.* **8**, 1026–1038 (2023).
57. Létoffé, S. et al. *Pseudomonas aeruginosa* production of hydrogen cyanide leads to airborne control of *staphylococcus aureus* growth in biofilm and in vivo lung environments. *mBio* **13**, e0215422 (2022).
58. Wang, J., Yu, B., Tian, D. & Ni, M. Rhamnolipid but not motility is associated with the initiation of biofilm seeding dispersal of *Pseudomonas aeruginosa* strain PA17. *J. Biosci.* **38**, 149–156 (2013).

59. Liu, D. et al. A library of promoter-*gfp* fusion reporters for studying systematic expression pattern of cyclic-di-GMP Metabolism-Related Genes in *Pseudomonas aeruginosa*. *Appl. Environ. Microbiol.* **89**, e0189122 (2023).
60. Miller, W. G., Leveau, J. H. & Lindow, S. E. Improved *gfp* and *inaZ* broad-host-range promoter-probe vectors. *Mol. Plant Microbe Interact.* **13**, 1243–1250 (2000).
61. Wurtzel, O. et al. The single-nucleotide resolution transcriptome of *Pseudomonas aeruginosa* grown in body temperature. *PLoS Pathog.* **8**, e1002945 (2012).
62. Sun, S. et al. Characterization of the multiple molecular mechanisms underlying RsaL control of phenazine-1-carboxylic acid biosynthesis in the rhizosphere bacterium *Pseudomonas aeruginosa* PA1201. *Mol. Microbiol.* **104**, 931–947 (2017).

Acknowledgements

We thank Dr. Yao Wu at Institute of Microbiology, Chinese Academy of Sciences for MST technical support. We thank the staffs from BL19U1 beamlines of National Facility for Protein Science in Shanghai (NFPS) at Shanghai Synchrotron Radiation Facility for their assistance during data collection. This work is supported by the National Key Research and Development Program of China (2021YFA0909500 to L.M. and F.L), the Strategic Priority Research Program of the Chinese Academy of Sciences (XDB0810000), the National Natural Science Foundation of China (32200149 to Y.Z[1]., 92351302 and 91951204 to L.M., 32070033 to D.W.), and the International Partnership Program of the Chinese Academy of Sciences Grant (079GJHZ2023029MI to L.M.).

Author contributions

Zhaoxiao Yu (Z.Y.), investigation, bacterial assays, writing–review & editing; Zhikun Wu, Yu Wei, Wei Huang and Feng Long (F.L.) contributes to the protein crystal structure analysis, writing– review & editing of the manuscript. Yu Zhang (Y.Z[1].), and Yaqian Zheng (Y.Z[2].), contributes to cell culture, infection, and antibiotic sensitivity analysis. Y.Z[1]., Haoyu Liu, Dejian Liu (D.L.), Yanhong Huang, Shumin Liao and Liang Li contributes to animal models, histopathological analyzes, and manuscript revision. Zhenyu Zhang, Xi Liu, Di Wang (D.W.), and Haiying Yu (H.Y.) contribute to the review and revision of the manuscript. Luyan Z. Ma (L.M.), conceptualization, supervision, fundings acquisition, and writing– review & editing of the manuscript. L.M., F.L., D.W., H.Y., Y.Z[1]. all contribute on the acquisition of funding.

Competing interests

Two Chinese patent applications have been filed based on the results of this manuscript: No#202310675915.1 (L.M., Y.Z., H.Y., D.W.) and No#202411253300.0 (L.M., Y.Z., Y.Z[1]., D.L., Y.Z[2]., H.Y., D.W.). The remaining authors declare no competing interests.

Additional information

Supplementary information The online version contains supplementary material available at https://doi.org/10.1038/s41467-025-57294-8.

Correspondence and requests for materials should be addressed to Feng Long or Luyan Z. Ma.

Peer review information *Nature Communications* thanks Henrietta Venter, and the other, anonymous, reviewer(s) for their contribution to the peer review of this work. A peer review file is available.